Impairment Mitigation in Long-Haul Optical Communication Links Employing Coherent Optical Orthogonal Frequency Division Multiplexing

A Project Report

submitted by

ANIRUDH VIJAY

in partial fulfilment of the requirements
for the award of the degree of

BACHELOR AND MASTER OF TECHNOLOGY

DEPARTMENT OF ELECTRICAL ENGINEERING
INDIAN INSTITUTE OF TECHNOLOGY MADRAS.

May 2019

THESIS CERTIFICATE

This is to certify that the project report titled **Impairment Mitigation in Long-Haul Optical Communication Links Employing Coherent Optical Orthogonal Frequency Division Multiplexing**, submitted by **Anirudh Vijay**, to the Indian Institute of Technology, Madras, for the award of the degree of **Bachelor and Master of Technology**, is a bona fide record of the research work done by him under our supervision. The contents of this report, in full or in parts, have not been submitted to any other Institute or University for the award of any degree or diploma.

Prof. Deepa Venkitesh
Research Guide
Associate Professor
Dept. of Electrical Engineering
IIT-Madras, 600 036

Prof. R. David Koilpillai
Research Guide
Professor
Dept. of Electrical Engineering
IIT-Madras, 600 036

Place: Chennai

Date: 5th May 2019

ACKNOWLEDGEMENTS

I would like to express my sincere gratitude to my research guides, Prof. Deepa Venkitesh and Prof. R. David Koilpillai for their constant support, patience and timely advice, technical and otherwise. It was Prof. Koilpillai's classes which built my foundation of digital signal processing and communication and Prof. Venkitesh's classes which gave me broad and deep understanding of photonics, nonlinear optics and optical communication. They were an integral factor in my choosing optical communication as my field of research for which I would forever be grateful.

My heartfelt thanks to Lakshmi Narayanan V who was my mentor in the lab and was with me throughout the project. The blind phase noise algorithm in this report was the collective work of the both of us. He introduced me to the techniques of digital signal processing for optical communication and I thank him for the numerous discussions on key concepts of optical communications and the simulations. I would also take this opportunity to thank Karthik Vijay A M who was my friend, classmate, mentor and advisor for not just the duration of the project but throughout my entire journey at IITM. His inputs for the simulations on nonlinear compensation were invaluable. I also thank my lab mates, especially Aneesh Sobhanan, for stimulating discussions and enriching my project experience.

I would like to extend my deep gratitude to my friends and classmates who made my life at IITM a memorable experience.

Last but not the least, I offer my earnest gratitude to my parents, sister and family for their constant emotional support and encouragement, for imparting strong moral values into me, and for providing the best education.

ABSTRACT

KEYWORDS: CO-OFDM; Optical Communication; CPE estimation; MSSI; SOA.

Due to the increasing demand for higher data rates, spectrally efficient transmission schemes like optical OFDM are gaining popularity. Coherent optical OFDM (CO-OFDM) leverages the advantage of the high receiver sensitivity of coherent detection and spectral efficiency of OFDM. The challenges in implementing CO-OFDM lie in mitigating the various impairments that originate at different stages of the transmission - at the transmitter, channel and receiver. This report focuses on the mathematical framework of CO-OFDM, the common impairments and ways to mitigate them. As a special case, fiber nonlinearity and chromatic dispersion using mid-span spectral inversion using SOA is presented.

TABLE OF CONTENTS

LIST OF TABLES

LIST OF FIGURES

ABBREVIATIONS

ASE	Amplified Spontaneous Emission
AWGN	Additive White Gaussian Noise
BER	Bit Error Ratio
CD	Chromatic Dispersion
CDC	Chromatic Dispersion Compensation
CFO	Carrier Freuqency Offset
CO-OFDM	Coherent Optical Orthogonal Frequency Division Multiplexing
CR	Clipping Ratio
CPE	Common Phase Error
DC	Direct Current, the zero frequency component of a signal
DFT	Discrete Fourier Transform
EVM	Error Vector Magnitude
FDE	Frequency Domain Equalizer
FFT	Fast Fourier Transform
FWM	Four-Wave Mixing
HNLF	Highly Non-Linear Fiber
ICI	Inter-Carrier Interference
IDFT	Inverse Discrete Fourier Transform
IFFT	Inverse Fast Fourier Transform
IQ	In-phase and Quadrature
K4P	Blind CPE estimation using Multilevel QPSK partitioning and Kalman filter
MDM	Mode Division Multiplexing
MIMO	Multiple Input Multiple Output
ML	Maximum Likelihood
MSSI	Mid Span Spectral Inversion
NLSE	Non-Linear Schrodinger Equation
OFDM	Orthogonal Frequency Division Multiplexing
OPC	Optical Phase Conjugation

OSNR	Optical Signal to Noise Ratio
PA	Pilot Aided
PAPR	Peak to Average Power Ratio
PDM	Polarization Division Multiplexing
PDL	Polarization Dependent Loss
PMD	Polarization Mode Dispersion
PM	Polarization Multiplexing
QAM	Quadrature Amplitude Modulation
QPSK	Quadrature Phase Shift Keying
RF	Radio Frequency
SINR	Signal to Interference plus Noise Ratio
SNR	Signal to Noise Ratio
SOA	Semiconductor Optical Amplifier
SSFM	Split Step Fourier Method
WDM	Wavelength Division Multiplexing

NOTATION

β_n	nth order derivative of wavenumber $\beta(\omega)$
j	Imaginary unit, $\sqrt{-1}$
ω_0	Centre frequency or carrier frequency
α	Coefficient of fiber attenuation
γ	Coefficient of fiber nonlinearity
W	DFT matrix
W	Dispersion parameter of fiber
T_s	Duration of an OFDM symbol
E_s	Energy of signal per information symbol
γ_p	Fraction of differential PDL
τ_{IQ}	IQ skew
L	Length of transmission
$\Delta\nu$	Linewidth of laser
$\mathcal{N}(\mu, \sigma^2)$	Normal (Gaussian) probability distribution with mean μ and variance σ^2
N_p	Number of pilot subcarriers
p	Number of polarizations used for transmission
$N_{\textbf{FFT}}$	Number of subcarriers, FFT size
$N_{\textbf{Filled}}$	Number of subcarriers carrying data/pilot symbols
Γ_{dB}	PDL coefficient in dB
T_0	Sampling interval
τ_c	SOA carrier lifetime
$P_{\textbf{sat}}$	SOA saturation power
α_{LW}	SOA linewidth enhancement factor
ϵ_{ch}	SOA carrier heating nonlinear gain supression factor
ϵ_{ch}	SOA spectral hole burning nonlinear gain supression factor
α_{ch}	SOA carrier heating gain phase coupling factor
c	Speed of light in vacuum
R_s	Total available bandwidth, symbol rate
$\mathbf{h}$	Vector of channel impulse response taps
$\mathbf{H}$	Vector of DFT of $\mathbf{h}$, sampled channel frequency response
$\mathbf{X}$	Vector of input symbols to the OFDM system
$\mathbf{x}$	Vector of time domain OFDM signal
λ	Wavelength

CHAPTER 1

INTRODUCTION

Orthogonal frequency division multiplexing (OFDM) and its variants have emerged as the leading modulation technique in wireless communication in the past decades (Nee and Prasad (2000)). It is a special type of multicarrier modulation where data is carried by multiple sub-carriers. The ability of OFDM to handle dispersion using single tap equalization in frequency selective fading channels and achieve capacity through waterfilling has made it the modulation of choice in wireless local area networks (WLAN), fourth generation (4G) and the upcoming fifth generation (5G) broadband cellular systems.

OFDM has also been extensively analysed in optical communication systems. While it debuted in optical wireless transmission (Tanaka *et al.* (2001)) and in multimode fiber systems to handle intermodal dispersion (Lowery and Armstrong (2005)), it was soon adapted into coherent optical systems (Shieh and Athaudage (2006)) to combat chromatic dispersion. After the advent of high bandwidth receivers with digital signal processing capabilities and rapid advances in wavelength division multiplexing, coherent detection has become the successor of intensity modulated direct-detection systems in long-haul optical communication due to its increased receiver sensitivity and higher degrees of freedom leading to longer reach and higher data rates. In the context of coherent optical communication, coherent optical orthogonal frequency division multiplexing (CO-OFDM) is seen as a contender for the next generation systems along with Nyquist wavelength division multiplexing (Nyquist-WDM) due to their high spectral efficiency (Bosco *et al.* (2010)). Spectral efficiency of 14 bit/s/Hz in a 400 Gbps, 256-QAM, 8192 subcarrier, 5 channel CO-OFDM transmission has been reported by (Omiya *et al.* (2013)). Long haul systems with 8000 km of transmission employing 1 Tbps, QPSK, 4096 subcarrier, 16 channel, unique-word DFT-spread CO-OFDM have been demonstrated by (Li *et al.* (2012)). The advantage of high spectral efficiency has also motivated the study of OFDM for passive optical networks (Qian *et al.* (2010)) and short reach communications (Dong *et al.* (2016)). For short transmission lengths, chromatic dispersion and polarization mode dispersion can be handled with the cyclic prefix

construct. However, for long-haul transmission, the challenges are different. OFDM is inherently sensitive to nonlinearity of any kind - fiber nonlinearity, frequency and timing errors and phase noise (Shieh and Djordjevic (2009)). The complexity of the receiver is proportionally high in order to tackle these challenges. The motivation of this project is to study the structure of a CO-OFDM system and investigate the challenges involved in realizing it practically in an optical communication system.

In this report, various impairments in a typical CO-OFDM system are studied and ways to mitigate the impairments and improve performance are discussed. The organization of the report is as follows:

Chapter 2 presents the construction of a typical OFDM system. The mathematical description of the building blocks of an OFDM system - modulation, demodulation, cyclic prefix and equalization. The chapter also discusses the realization of single polarization CO-OFDM and polarization division multiplexed CO-OFDM. The AWGN performance is studied through simulations. The second part of the chapter focuses on common impairments in CO-OFDM systems at the transmitter, receiver and the channel and ways to mitigate them. The impairments considered are fiber nonlinearity and chromatic dispersion, carrier frequency offset, polarization dependent loss and laser phase noise. For chromatic dispersion and for carrier frequency offset, modulation transparent digital compensation techniques are discussed. For polarization dependent loss, polarization-time codes, a coding scheme inspired from wireless communications are used for mitigation. In the case of laser phase noise, a pilot aided technique and a novel blind technique are presented. The chapter also includes simulation results demonstrating the performance characteristics of the system along with the mitigation strategies. The final section of the chapter presents the hardware level impairments that are faced in practice.

Chapter 3 focuses on a special case of nonlinearity and chromatic dispersion compensation using Mid-span spectral inversion using semiconductor optical amplifier (SOA). SOA and its simulation model are presented in this chapter. The performance of MSSI for CO-OFDM is studied and compared with the unmitigated scheme.

Chapter 4 includes the conclusions and possible directions for future research in the topics discussed.

CHAPTER 2

COHERENT OPTICAL ORTHOGONAL FREQUENCY DIVISION MULTIPLEXING

The current 100 gigabit Ethernet standard uses $25\,GBaud$ polarization division multiplexed non return-to-zero (NRZ) QPSK signalling. The wavelength division multiplexed channels are spaced in a rigid grid with a 50 GHz spacing (van den Borne *et al.* (2009)) giving a spectral efficiency of 2 bit/s/Hz. Due to a shift towards flexible grid spacing in the next generation systems and increase in the demand of data rates, spectrally efficient modulations like CO-OFDM and Nyquist WDM are studied for suitability. In the current NRZ QPSK signalling, due to slow roll-off in the frequency domain, the grid spacing needs to be high. This requirement is relaxed in OFDM and the signal bands can be brought closer, improving the spectral efficiency. In this chapter, the description of CO-OFDM, common impairments in a CO-OFDM system and methods to mitigate them are presented.

2.1 System description of OFDM

The typical structure of an OFDM transmitter and an OFDM receiver are shown in figures 2.2, 2.3 (Armstrong (2009)). In OFDM, as the name suggests, the available frequency band R_s is broken into small sub-bands called subcarriers. Each subcarrier has a power spectrum of the form $\text{sinc}^2(x)$ and its spectrum overlap with that of the neighbouring subcarriers. However, the subcarriers are carefully spaced so that the peaks of each of the $\text{sinc}(x)$ spectra falls on the nulls of the spectra of the other subcarriers. Thus, when the frequency domain is sampled at these points, there will be no inter-carrier interference (ICI).

An advantage of OFDM is that the modulation can be digitally realized using the inverse discrete Fourier transform (IDFT) or the discrete Fourier transform (DFT) operation. The eigen vectors of DFT are naturally orthogonal. The DFT operation takes

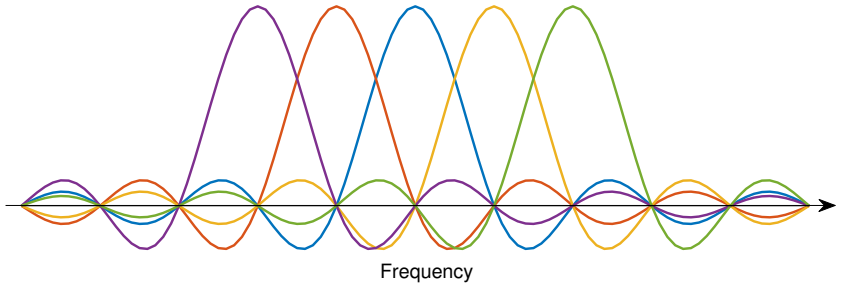

Figure 2.1: Spectrum of an OFDM signal showing the sinc(x) shaped subcarriers.

a discrete time sequence and produces a frequency representation which is the sampled version of the continuous periodic frequency representation of the discrete time sequence. Thus by using the IDFT operation the data can be modulated onto orthogonal carriers and by using the DFT operation the frequency domain can be sampled and the data can be retrieved from the carriers. Note that IDFT and IFFT are interchangeably used. Strictly speaking IFFT is an algorithm to efficiently implement the mathematical operation IDFT. Similarly, DFT and FFT are interchangeably used.

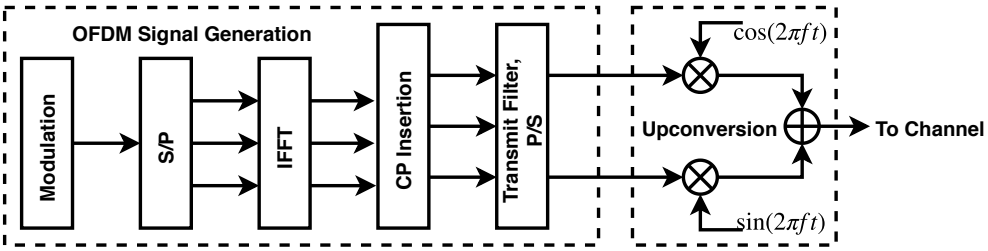

Figure 2.2: Schematic of OFDM transmitter. S/P - Serial to Parallel, P/S - Parallel to Serial, f is the carrier frequency.

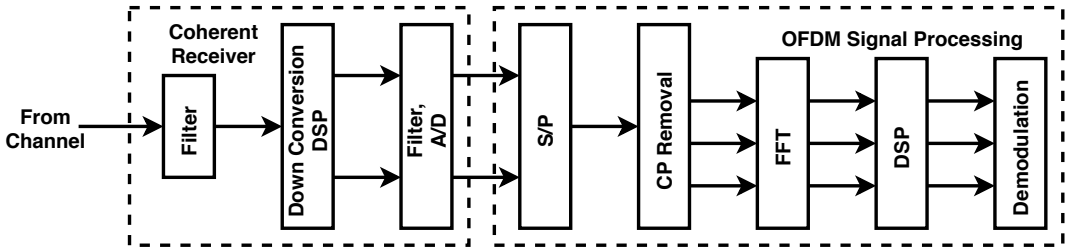

Figure 2.3: Schematic of OFDM Receiver. S/P - Serial to Parallel, A/D - Analog to Digital, DSP - Digital Signal Processing.

With the unique structure of OFDM having independent frequency components,

channel equalization is efficiently performed on each subcarrier independently. The block transceiver structure of OFDM processes data in blocks. By using the IDFT/DFT framework, intra block interference (eg. ICI) has been eliminated. Channel frequency selectivity can still result in inter block interference. A cyclic prefix (CP) is attached to every block to absorb the dispersive leakage from the previous block. The cyclic prefix is inserted at the transmitter and removed at the receiver before processing. These two frameworks, namely the IDFT/DFT and the cyclic prefix, ensure simple channel equalization in OFDM systems. At the OFDM transmitter (figure 2.2), the bits are mapped to complex M-QAM symbols which are then loaded into the subcarriers using the IFFT operation. Then, the cyclic prefix is inserted and the signal converted to the analog domain and up-converted for transmission. At the receiver (figure 2.3), the received signal is filtered to remove out-of-band noise and downconverted and digitized to obtain the sampled base-band signal. The OFDM signal processing undoes all the operations at the transmitter - cyclic prefix removal, FFT, DSP for correcting impairments and demapping from complex symbols to bits.

IDFT and DFT blocks IDFT and the DFT blocks are the key to digitally realizing OFDM. At the transmitter (optical OFDM or wireless OFDM), the OFDM signal generation consists of mapping bits to complex QAM constellations and serial to parallel (S/P) conversion before the IDFT operation (Figure 2.2). At the receiver, the DFT block transforms the information back to frequency domain before digital signal processing (like equalization) and demodulation (Figure 2.3). The complex data vector at the input of the IDFT block is denoted as $\mathbf{X} = [X_0, X_1, \ldots X_{N_{\text{FFT}}-1}]^T$. Here N_{FFT} is the order of IFFT and the number of subcarriers in total. X_l represents the data carried on the lth subcarrier. After the IDFT block, the signal is represented by the vector $\mathbf{x} = [x_0, x_1, \ldots, x_{N_{\text{FFT}}-1}]^T$.

$$x_l = \frac{1}{\sqrt{N_{\text{FFT}}}} \sum_{k=0}^{N_{\text{FFT}}-1} X_k \text{exp}\left(\frac{j2\pi kl}{N_{\text{FFT}}}\right) \tag{2.1}$$

for $l = 0, 1, \ldots, N_{\text{FFT}}$. $1/\sqrt{N_{\text{FFT}}}$ is the normalization factor to ensure a unitary transformation. We see that x_l is a linear combination of scaled complex sinusoids. The inverse

relationship to obtain $\mathbf{X}$ from $\mathbf{x}$ is,

$$X_k = \frac{1}{\sqrt{N_{\text{FFT}}}} \sum_{l=0}^{N_{\text{FFT}}-1} x_l \text{exp}\left(-\frac{j2\pi kl}{N_{\text{FFT}}}\right). \tag{2.2}$$

This is the form of the demodulation block at the receiver after CP removal. If the complex vector $\mathbf{X}$ draws values from an M-QAM constellation, then there are $M^{N_{\text{FFT}}}$ combinations of the vector $\mathbf{x}$. Each element x_l in $\mathbf{x}$ is independent and identically distributed. As each x_l is a linear combination of X_k's, the probability density of x_l approaches a Gaussian as dictated by the central limit theorem. This is especially valid for large N_{FFT}. A sequence of samples from a tailed distribution like Gaussian tends to have large peak values. Thus the peak to average power ratio (PAPR) of an OFDM system is high. This affects the performance of OFDM systems that use devices with tight linear regimes like RF amplifiers and electro-optic modulators.

Cyclic prefix and single tap equalization For a block transmission scheme, we have to extend the notation to include the time axis. The complex symbols after S/P block can be expressed as a sequence of vectors $\mathbf{X}[n]$. This results in a sequence of vectors $\mathbf{x}[n]$ after the IDFT block. At the transmitter, the CP is inserted for each block. For input $\mathbf{x}[n] = [x_0[n], x_1[n], \ldots, x_{N_{\text{FFT}}-1}[n]]^T$, the CP insertion block yields,

$$\mathbf{x}_{CP}[n] = [x_{N_{\text{FFT}}-L_{\text{CP}}}[n], x_{N_{\text{FFT}}-L_{\text{CP}}+1}[n], \ldots, x_{N_{\text{FFT}}-1}[n], x_0[n], x_1[n], \ldots, x_{N_{\text{FFT}}-1}[n]]^T \tag{2.3}$$

where L_{CP} is the length of the CP. At the receiver the CP is discarded before processing. The CP length should at least be the RMS delay spread of the channel. By using the CP, the interference from the previous block is eliminated. The only interference due to channel selectivity is within the block. This is eliminated by using the FFT operation that leverages the orthogonality of the subcarriers. The orthogonality is undisturbed as the CP converts the linear convolution of the channel impulse response with $\mathbf{x}_{CP}[n]$ to circular convolution with $\mathbf{x}[n]$. A circular convolution with $\mathbf{x}[n]$ is a term by term multiplication of the frequency domain channel response and $\mathbf{X}[n]$. This enables simple single tap channel equalization. Denote the channel impulse response (sampled spaced) as $\mathbf{h} = [h_1, h_2, \ldots, h_{L_{\text{CP}}}]^T$ and its N_{FFT}-point FFT as $\mathbf{H} = [H_1, H_2, \ldots, H_{L_{\text{CP}}}]^T$. If the channel also adds AWG noise, then the baseband equivalent received signal is, $y_r[m] = h[m] * x_t[n] + w_r[n]$, where $x_t[n]$ is the baseband equivalent transmitted sequence after

P/S conversion, $w_r[n]$ is the AWG noise and $(*)$ denotes linear convolution. After S/P conversion (blocking operation) and CP removal, the signal becomes $\mathbf{y}[n] = \mathbf{h} \circledast \mathbf{x}[n] + \mathbf{w}[n]$, where the elements of $\mathbf{w}[n]$ have the same statistics as $w_r[n]$. After FFT operation, we have for $k = 0, 1, \ldots, N_{\text{FFT}} - 1$

$$Y_k[n] = H_k[n]X_k[n] + W_k[n]. \tag{2.4}$$

Due to the unitary nature of FFT operation, the elements of $\mathbf{W}[n]$ have the same statistics as $w_r[n]$. Equation (2.4) indicates that each channel is equivalently an AWGN channel - the channels are parallelized.

Peak to average power ratio and clipping The entire system from the transmitter to the receiver is assumed to be linear. This linearity is required for perfect modulation and demodulation of OFDM. Any nonlinearity will result in loss of orthogonality between the subcarriers and result in ICI. Sources of nonlinearity include the channel, oscillators, modulators and power amplifiers at the transmitter and receivers to name a few. OFDM signals have higher peak to average power ratio (PAPR) than single carrier signals using the same modulation. The power amplifiers in the system have finite linear regimes. Their operating conditions have strict peak-peak signal amplitude limitations. Due to high PAPR, to avoid nonlinearity the input average power to the amplifiers is limited. This reduces the SNR at the transmitter itself. Thus there is a trade-off between nonlinearity and average power in an OFDM system. Any channel side nonlinearity additionally contributes to this effect.

To limit the effect of nonlinearity, the signal amplitude is clipped in a controlled nonlinear fashion. The signal amplitude is digitally clipped while preserving the signal phase. Consider the complex analog baseband signal $x_a(t)$ corresponding to $x_{CP}[n]$.

$$x_{\text{clip}}(t) = \begin{cases} x_a(t) & x_a(t) \leq A \\ Ae^{j\arg\{x_a(t)\}} & x_a(t) > A. \end{cases} \tag{2.5}$$

The clipping ratio (CR) is defined as the ratio of the clipped amplitude and RMS amplitude.

$$\text{CR (dB)} = 20\log_{10}\left(\frac{A}{\sqrt{E|x_a(t)|^2}}\right) \tag{2.6}$$

Clipping should be done on the analog signal $x_a(t)$ or an upsampled (and interpolated) version of $x_{CP}[n]$ for it to be effective. This is because the digital to analog conversion may produce peaks in between sample points. While clipping reduces the PAPR, it increases the out-of-band power. Figure 2.4 shows this effect. The out-of-band leakage increases as the clipping ratio (peak power w.r.t the RMS power) decreases. This may cause interference with nearby OFDM bands.

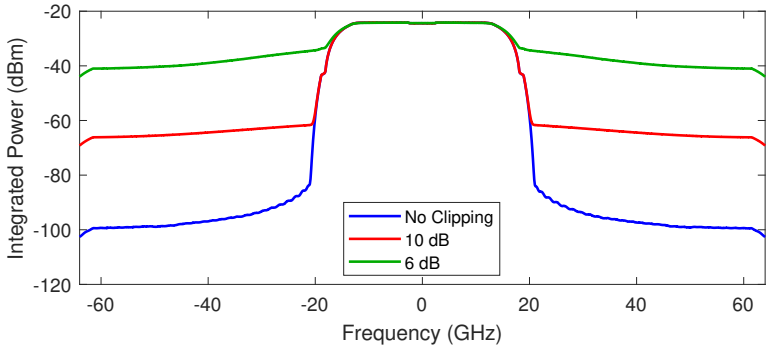

Figure 2.4: Effect of clipping on the power spectrum. The OFDM signal shown here has 32 $Gbaud$ baudrate

2.1.1 Realization of coherent optical OFDM

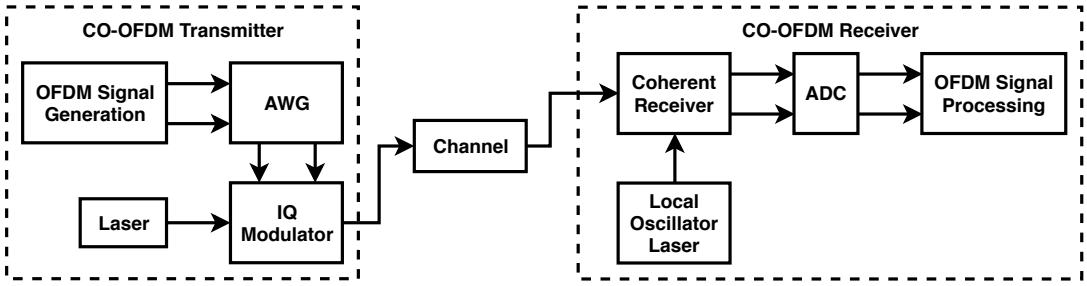

Figure 2.5: Schematic of CO-OFDM transmitter and receiver. AWG - Arbitrary Waveform Generator, ADC - Analog to Digital Converter

Coherent optical OFDM (CO-OFDM) is a linear modulation of OFDM onto the electric field of an optical carrier. The optical transmitter-receiver schematic for coherent OFDM is shown in figure 2.5. The OFDM signal is generated electrically as I (real) and Q (imaginary) components through an arbitrary waveform generator (AWG). These RF signals drive the I and Q arms of an IQ modulator with an optical input from a single mode laser (Tang *et al.* (2007)), refer figure 2.6. The Mach-Zehnder modulators in the

IQ modulator are null-biased to suppress the carrier. The phase modulator in one of the arms adds $\pi/2$ phase shift to ensure orthogonality between I and Q components. The electrical RF OFDM signal from the AWG is modulated on the optical carrier (laser). The IQ-modulator is equivalent to the upconverter in figure 2.2.

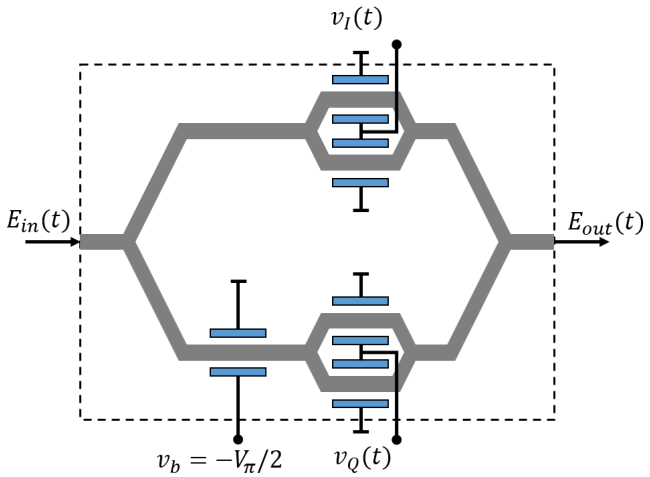

Figure 2.6: Structure of an optical IQ modulator. $E_{in}(t)$ and $E_{out}(t)$ are the optical input and output respectively, $v_I(t)$ and $v_Q(t)$ are the RF drive voltages corresponding to I and Q channels respectively.

At the receiver end, the signal is optically filtered to remove any out-of-band noise and fed into the coherent receiver. This is essentially a downconverter. The filtered optical signal is mixed with a local oscillator signal at the same carrier frequency as that of the transmitter. To obtain both I and Q components, the received signal is split and mixed with the local oscillator signal and its $\pi/2$ phase delayed copy. The mixed signals are received on a pair of balanced photodiodes whose photocurrents will carry both the phase and amplitude information of the modulated signal. This setup is called a 90°hybrid (Kazovsky *et al.* (1987)) and is used for coherent detection of optical signals. The photocurrents are sampled and digitized by the analog to digital converter (ADC) and fed into the OFDM signal processing block (refer figure 2.3).

Polarization division multiplexing

Time, amplitude and quadrature are three degrees of freedom that are typically exploited in coherent modulations. In a single mode fiber, the other degrees of freedom are wavelength and polarization states. Wavelength division multiplexing leverages the large bandwidth of the optical fiber channel. Polarization division multiplexing lever-

ages the two orthogonal states of polarization of the optical carrier to potentially double the transmission capacity. In current practice, polarization division multiplexing is combined with QAM modulation to transmit data faster than 100 Gbit/s over a single wavelength (Essiambre *et al.* (2010)).

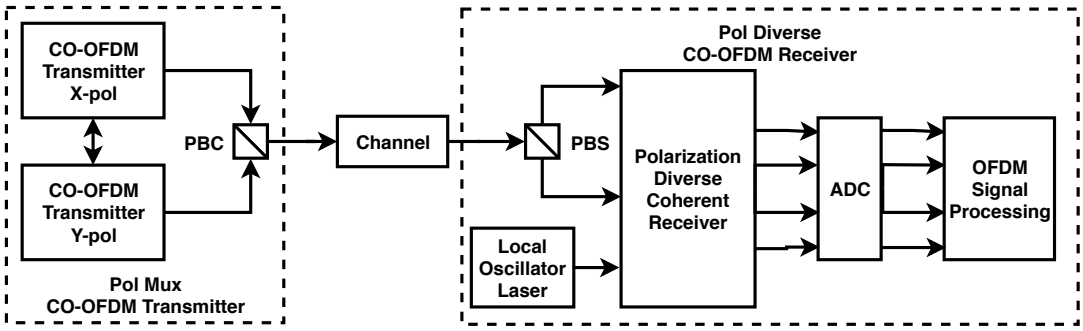

Figure 2.7: Schematic of PDM CO-OFDM transmitter and receiver. Pol Mux - Polarization Multiplexed, PBC - Polarization Beam Combiner, PBS - Polarization Beam Splitter, ADC - Analog to Digital Converter

The schematic of a polarization division multiplexed (PDM) CO-OFDM is rendered in figure 2.7. Two CO-OFDM transmitter are used to generate the X and Y polarization signals which are combined using a polarization beam combiner and then launched into the channel. The X and Y pol signals of the PDM CO-OFDM transmitter are synchronized. At the receiver end, a polarization beam splitter splits the two polarizations components. The coherent receiver contains two 90°hybrid structures to detect the I and Q components of both X and Y polarization. The signal processing module at the receiver handles these four quantities in parallel.

Elements of an CO-OFDM optical communication link

The three important parts of any communication link are the transmitter, the receiver and the channel. The following are the important components and parameters of a CO-OFDM fiber link:

1. Transmitter
    - Laser - power and linewidth
    - OFDM RF signal generation - OFDM parameters
    - IQ modulator - bandwidth, bias
    - Pre-amplifier - signal launch power

2. Fiber Optic Channel
    - Fiber - dispersion, nonlinearity, attenuation, polarization dependent loss
    - Inline amplifiers - gain, noise figure

3. Receiver
    - Local oscillator laser - power, linewidth, frequency offset
    - Receive filter - Optical filter bandwidth, electrical filter bandwidth

The performance of a CO-OFDM link with the above elements is studied in this report. Impairments at each stage are considered and ways to mitigate them investigated. The next section analyses the performance of a CO-OFDM system in an additive white Gaussian noise channel.

2.1.2 Performance of CO-OFDM systems in AWGN channels and simulation environment

From equation (2.4), we know that the channel is parallelized. If the channel is an AWGN channel, then $H_k = 1 \forall k \in \{0, 1, \ldots, N_{\text{FFT}} - 1\}$. Therefore the BER performance of an M-QAM CO-OFDM system is similar to the bit error rate (BER) performance of a single carrier M-QAM system. However, due to the possibility of partially filled bandwidth, there will be an additional factor of $N_{\text{filled}}/N_{\text{FFT}}$ in the SNR expression. The OSNR of the CO-OFDM system is given as (Shieh and Djordjevic (2009)),

$$\text{OSNR} = p \times \frac{R_s}{2B_{\text{ref}}} \times \text{SNR} = p \times \frac{R_s}{2B_{\text{ref}}} \times \frac{N_{\text{Filled}}}{N_{\text{FFT}}} \times k \times \frac{E_b}{N_0} \tag{2.7}$$

where p is the number of polarizations used for communication, R_s is the symbol rate and the total bandwidth available for OFDM, B_{ref} is the noise reference bandwidth (usually corresponds to 0.1 nm as reference in optical communication systems), N_{Filled} and N_{FFT} are the number of filled subcarriers and the total number of subcarriers respectively, k is the number of bits per symbol of the complex data in the subcarriers, E_b is the signal power per bit and N_0 is the noise spectral density. From E_b/N_0, the approximate BER performance in AWGN can be analytically estimated (see table 2.1) (Proakis (2001)). The error vector magnitude (EVM) is also a metric of performance and is defined as,

$$\text{EVM} = \sqrt{\frac{||\mathbf{x} - \mathbf{x}_0||^2}{E||\mathbf{x}_0||^2}} = \frac{1}{\sqrt{\text{SNR}}} \tag{2.8}$$

where $\mathbf{x}$ is the vector of received constellation points and $\mathbf{x}_0$ is the vector of transmitter constellation points.

Table 2.1: BER and E_b/N_0 relationship for different Modulation formats

Modulation Format	k	Approximate BER
QPSK (4 QAM)	2	$\frac{1}{2}\text{erfc}\left(\sqrt{\frac{E_b}{N_0}}\right)$
16 QAM	4	$\frac{3}{8}\text{erfc}\left(\sqrt{\frac{4E_b}{10N_0}}\right)$
64 QAM	6	$\frac{2}{3}\text{erfc}\left(\sqrt{\frac{18E_b}{63N_0}}\right)$

Simulations

All simulations in this report are run in MATLAB simulation environment using the Optilux package (Serena (2009)). Optilux is an open-source package to simulate and analyze optical communication systems. It includes optimized codes for the simulation of optical devices used in optical communication like modulators and amplifiers and modules for numerically solving signal propagation in a fiber. In all simulations, timing synchronization is assumed to be perfect. BER performance of a PM CO-OFDM system with AWGN channel is studied through simulations. The relevant simulation parameters are given in the table 2.2. These parameters are chosen according to the hardware available in the optical communication laboratory at IITM. The signal generator at the transmitter, the optical modulator and the ADC at the receiver are suitable for a $32\,Gbaud$ transmission.

Table 2.2: CO-OFDM parameters for simulation: AWGN Performance

Parameter	Value
Symbol Rate R_s	$32\,Gbaud$
Modulation	16 QAM
FFT size N_{FFT}	128
OFDM symbols N_{symb}	512
Filled Bandwidth	$25.6\,GHz$
PRBS order	15

Figure 2.8 shows the simulated spectra of the X and Y polarization components of the CO-OFDM signal and the BER performance in AWGN. The system is ideal but

for the noise addition. The close agreement between the theoretical and the simulated performance curves indicates that the simulation conditions are optimal.

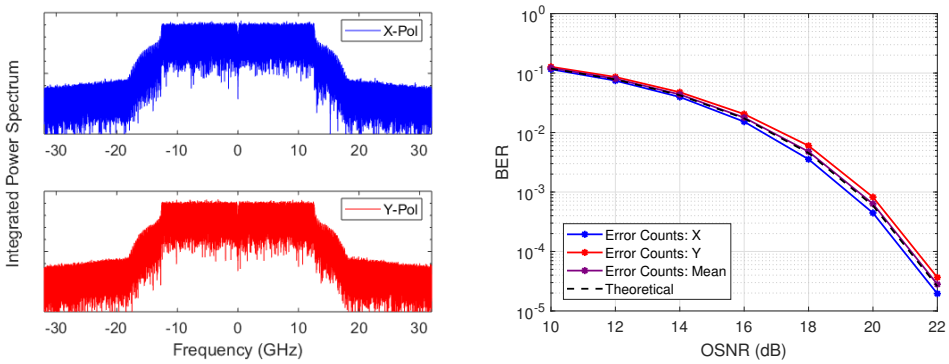

Figure 2.8: Simulation of CO-OFDM system in Optilux: Spectra of X and Y polarization components of CO-OFDM signal (left) and the BER performance in AWGN system (right)

2.2 Common impairments in CO-OFDM systems

This section discusses common impairments found in any CO-OFDM systems. The impairments could be at the transmitter, receiver or due to the channel.

2.2.1 Nonlinearity and chromatic dispersion

An optical fiber channel is nonlinear and dispersive in nature (Agrawal (2012)). The dispersion is due to the differential speeds (due to different effective refractive indices) with which every frequency component of the electric field travels in the medium. This dispersion causes intersymbol interference. The fiber nonlinearity (Kerr nonlinearity) (Agrawal (2012)) arises from the interaction of electric field components with the medium to generate third order products. Mathematically, this is due to the dependence of the electric susceptibility of the medium on the electric field. Nonlinearity and chromatic dispersion are both introduced in the channel simultaneously and hence are coupled. Optimally, these have to be compensated simultaneously (Ip and Kahn (2008)). However, in the low power regime ($< 0\,dBm$), nonlinearity is weak and chromatic dispersion dominates.

The Nonlinear Schrodinger Equation (NLSE) governs pulse propagation in a fiber.

It establishes the spatial and temporal relationship between the electric field envelope and the medium. It is derived from Maxwell's equations. Considering the time variable T and space variable z, the evolution of the electric field envelope $A = A(T, z)$ is given by (Agrawal (2012)),

$$\frac{\partial A}{\partial z} + j\frac{\beta_2}{2}\frac{\partial^2 A}{\partial T^2} - j\gamma|A|^2 A + \frac{\alpha}{2}A = 0 \tag{2.9}$$

where $\beta_2 = \frac{\partial^2 \beta}{\partial \omega^2}\big|_{\omega_0}$ is the coefficient of $(\omega - \omega_0)^2$ the expansion of the wavenumber $\beta(\omega)$ about ω_0 with units ps^2/km, γ is the coefficient of nonlinearity with units W^{-1}/km and α is the attenuation constant with units $Np.km^{-}1$. A in in units $\sqrt{W}$. The terms in equation 2.9 denote, from left to right, the spatial variation of the envelope, the group velocity dispersion, the fiber nonlinearity and attenuation respectively. The equation has been written in the frame of reference of the pulse, $T = t - \beta_1 z$, where $\beta_1 = \frac{\partial \beta}{\partial \omega}\big|_{\omega_0}$ is the group velocity.

For low launch powers, the term $j\gamma|A|^2 A$ is neglected and the NLSE simplifies to

$$\frac{\partial A}{\partial z} + j\frac{\beta_2}{2}\frac{\partial^2 A}{\partial T^2} + \frac{\alpha}{2}A = 0 \tag{2.10}$$

which can be solved in the Fourier domain. Taking $\Omega = \omega - \omega_0$, we have

$$\frac{\partial A(\Omega, z)}{\partial z} - j\frac{\beta_2}{2}\Omega^2 A(\Omega, z) + \frac{\alpha}{2}A(\Omega, z) = 0 \tag{2.11}$$

The solution to the above equation is,

$$\begin{aligned} A(\Omega, L) &= A(\Omega, z = 0)\text{exp}\left(j\frac{\beta_2}{2}\Omega^2 L - \frac{\alpha}{2}L\right) \\ &= A(\Omega, z = 0)F_L\text{exp}\left(j\frac{\beta_2}{2}\Omega^2 L\right) \end{aligned} \tag{2.12}$$

where $F_L = \exp\left(-\frac{\alpha}{2}L\right)$ is the amplitude attenuation. In chapter 3, nonlinearity and chromatic dispersion mitigation using nonlinear optics is discussed. The next section will deal with digital chromatic dispersion compensation.

Frequency domain equalization of chromatic dispersion

Chromatic dispersion being a linear impairment, the fiber can be approximated as a linear time-invariant (LTI) channel with frequency response $H_{CD}(j\Omega)$. From NSLE equation, neglecting nonlinearity and attenuation, $H_{CD}(j\Omega) = e^{j\frac{\beta_2}{2}\Omega^2 L}$, which is an all-pass filter with a quadratic frequency dependent phase. Here, L is the length of transmission in the fiber. In an OFDM system, with cyclic prefix of sufficient length, chromatic dispersion can be mitigated using single-tap equalization. However, in high speed long-haul systems, the cyclic prefix overhead can be large. For instance, consider a 128 subcarrier, $20\,GBaud$ OFDM signal. Without cyclic prefix the length of one OFDM symbol is $6.4\,ns$. For a 1000 km transmission over a fiber with dispersion parameter $D = 17ps/nm.km$ and carrier wavelength $\lambda_0 = 1550\,nm$, the dispersive spread is approximately $D \times L \times \Delta\lambda = 2.72\,ns$ ($\Delta\lambda$ is the linewidth of the spectrum in nm) which should be the minimum length of the cyclic prefix. This corresponds to an overhead of about 30%.

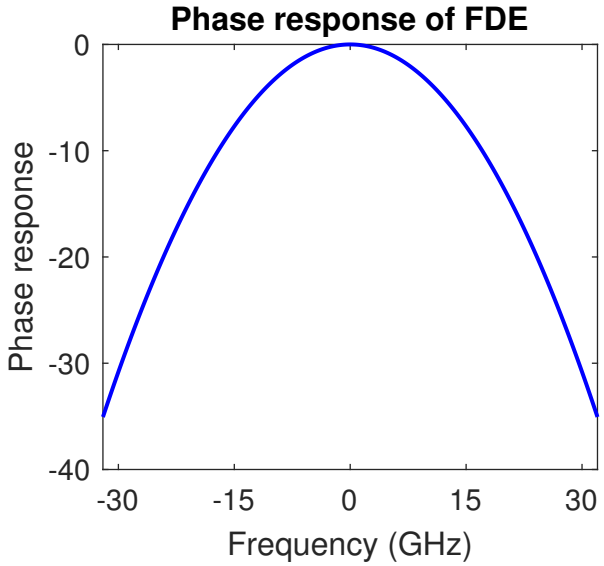

Figure 2.9: Frequency Domain Equalizer phase transfer function: The phase response is for $\beta_2 = -20\,ps^2/km$ and 80 km transmission.

As second order dispersion is a deterministic impairment, frequency domain equalization can be used. The equalization filter is simply the inverse phase function $H_{CD}(j\Omega)$ sampled at the desired digital frequencies. The equalization can be realized as a point-

to-point multiplication after DFT operation on the received signal vector $\boldsymbol{y}$.

$$\begin{aligned} H(f_k) &= H^*_{CD}(j2\pi f_k) \\ H_{FDE} &= \text{diag}\{H(f_k)\} \\ \boldsymbol{y_{CD}} &= W^{-1} H^*_{FDE} W \boldsymbol{y} \end{aligned} \tag{2.13}$$

where W is the DFT matrix and $\{f_k\}$ are the frequencies of the DFT spectrum of $\boldsymbol{y}$. $\boldsymbol{y}_{CD}$ is the CD equalized signal. Figure 2.9 shows the FDE phase response required for a $20\,Gbaud$ CO-OFDM propagating through one span of 80 km SSMF with dispersion parameter $D = 17\,ps/nm.km$. The dispersion parameter D is related to β_2 as $D = -2\pi c\beta_2/\lambda^2$. The efficacy of CD compensation can be seen in the constellation diagrams of figure 2.10. The CP aided channel equalization based CD compensation uses a CP of length 10. This is sufficient for 80 km transmission. The performance of this method is poorer because the frequency resolution of the equalization is not sufficient and increasing N_{FFT} will help improve the performance.

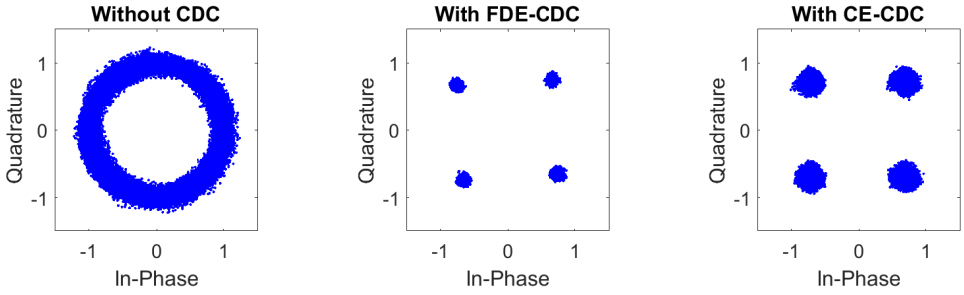

Figure 2.10: Constellation diagrams of a QPSK CO-OFDM signal at the demodulation stage without (left) any CD compensation, with frequency domain equalization (middle) and with channel equalization (CE) and CP construct (right).

As chromatic dispersion is an infinite impulse response filter, the efficiency of the FDE improves with the frequency resolution of the DFT operation, or in other words, the length of the time window. However, this may be very computationally expensive and result in latency in real time implementations. Thus in practice, the FDE is performed using standard techniques like overlap-add and overlap-save techniques (HARRIS (1987)).

2.2.2 Carrier frequency offset

Carrier frequency offset (CFO) is a receiver side impairment in every coherent system using a heterodyne receiver. Heterodyne means that the local oscillator laser at the receiver is independent of the laser at the transmitter. The frequency offset, as the name suggests, is the offset between the centre frequencies of the lasers at the transmitter and the receiver. Even though both of these lasers are designed to oscillate at the same optical frequency, due to practical reasons, there will be a small non-zero offset typically less than 1 GHz for industry grade lasers.

Uncompensated frequency offset results in phase accumulation and subsequent failure in data retrieval. Consider the received optical signal $y(t)$ of the form in terms of the centre frequency of the transmit laser Ω_{tx},

$$y(t) = x(t)\exp\left(j\Omega_{tx}t\right). \tag{2.14}$$

At the local oscillator, the received optical signal is mixed with the local oscillator signal with centre frequency Ω_{rx} and power P_{LO}. The receiver output (in the complex baseband equivalent form) is given as,

$$y_{mixer}(t) = x(t)\sqrt{P_{LO}}\exp\left(j\left(\Omega_{tx} - \Omega_{rx}\right)t\right). \tag{2.15}$$

In the ideal case, $\Delta\Omega = \Omega_{tx} - \Omega_{rx} = 0$ and the output is proportional to the baseband signal. However for nonzero $\Delta\Omega$, the output has an extra time varying phase, $\Delta\Omega t$, which affects the demodulation of the complex data in $x(t)$. In the case of OFDM, such a frequency offset will break the orthogonality of the subcarriers. In the following section, the periodogram technique to estimate and correct the frequency offset.

Periodogram technique to mitigate frequency offset The periodogram technique is a digital frequency domain method to estimate the frequency offset. It involves performing repeated convolution on the frequency spectrum with itself to obtain a peak corresponding to the frequency offset.

Consider the (scaled) oversampled received signal with sampling interval T_0,

$$r[n] = e^{j2\pi\Delta\Omega nT_0}x[n] \tag{2.16}$$

To estimate the offset, the received signal is raised to the power 4.

$$(r[n] - E\{r[n]\})^4 = \left(e^{j2\pi\Delta\Omega nT_0}x[n] - E\{e^{j2\pi\Delta\Omega nT_0}x[n]\}\right)^4 \tag{2.17}$$

where the mean is subtracted to avoid getting a peak at DC. The frequency offset is the estimated by computing the DFT of the above quantity and finding the frequency corresponding to the highest peak.

$$\begin{aligned} P(f_k) &\triangleq \mathscr{F}_{DFT}\{\left(e^{j2\pi\Delta\Omega nT_0}x[n] - E\{e^{j2\pi\Delta\Omega nT_0}x[n]\}\right)^4\} \\ f_{peak} &= \arg\max_{f_k} |P(f_k)| \\ \hat{\Delta\Omega} &= f_{peak}/4 \end{aligned} \tag{2.18}$$

where $\{f_k\}$ form the frequency axis of the spectrum. Frequency offset can be corrected by digitally subtracting a linearly increasing phase corresponding to the estimated offset.

$$\hat{r}_{LO}[n] = r[n]e^{-j2\pi\hat{\Delta\Omega}nT_0} \tag{2.19}$$

Figure 2.11 depicts the working of the periodogram technique for different CFO value - the peak of the spectrum of the fourth power of the signal is used to obtain the frequency offset. The simulated OFDM system operates at $20\,Gbaud$ and the sampling rate is $60\,GS/s$ (oversampling factor 3). The correction factor in equation (2.19) does not result in noise amplification. This is the reason why AWG noise was not considered in the received signal. In reality, noise affects the accuracy of the estimate of CFO and the method fails at low OSNR.

The algorithm requires the signal to be sufficiently oversampled. The maximum measurable offset depends on the oversampling factor. The nonlinear fourth power operation in equation (2.18) imposes the condition that the maximum offset must be less than one-fourth of the maximum frequency represented by the DFT operation.

$$\Delta\Omega < \frac{1}{8T_0}. \tag{2.20}$$

Furthermore, the accuracy of the estimate depends on the frequency resolution of the DFT spectrum. A larger window of $r[n]$ will improve the accuracy of the estimate. However, this will increase the latency of real time CFO estimation. In practice, as

the frequency offset can vary slowly with time, a new estimate is computed once every OFDM block.

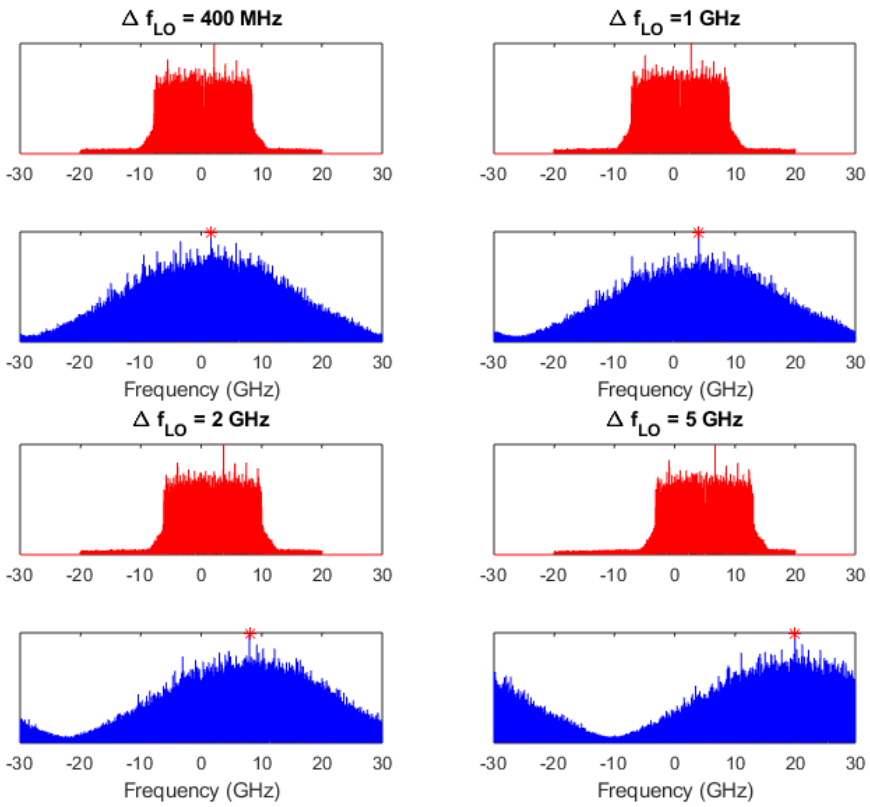

Figure 2.11: Frequency Offset compensation using the periodogram technique. The spectra in red correspond to $r[n]$ and the spectra in blue correspond to $P(f_k)$. The peaks of $P(f_k)$ are marked with red asterisks and correspond to four times the respective frequency offsets.

2.2.3 Polarization dependent loss

To meet the demands of increasing capacity (Winzer (2012)), all physical dimensions of the optical channel have to be exploited. Polarization is one such dimension where multiplexing can be used to double the capacity. In polarization division multiplexing information is encoded on the two orthogonal polarizations (X and Y) of the optical carrier (refer section 2.1.1). These polarization division multiplexed systems potentially increase the capacity by a factor of 2. This increase in spectral efficiency can be achieved only if the associated problems of polarization mode dispersion (PMD) and polarization dependent loss (PDL) (Gordon and Kogelnik (2000),Duthel *et al.* (2008),Juarez *et al.* (2012)) are dealt with. The former causes a differential delay between the components of X and Y polarizations and in the context of OFDM systems it can be mitigated by

using sufficient cyclic prefix. The latter, PDL, causes differential losses between the two orthogonal polarizations. In a long haul link, there are many sources of PDL: amplifiers, couplers, filters to name a few. Though the individual contribution of any one device is low, the cumulative effect can still affect the system performance. Additionally this impairment is time-varying and stochastic in nature. Drawing parallels from similar channels in wireless communications, this effect can be modeled as fading in a Multiple-Input Multiple-Output (MIMO) system (Shieh *et al.* (2007)). In a traditional, uncoded transmission scheme, the data and the transmitted signal in each polarization is independent. The time-varying fluctuations in OSNR in the two polarizations, due to the differential gain, cause a fading like effect. If there is a fading event that results in a severe deterioration of OSNR in one of the polarizations, the data in that polarization cannot be recovered. The established digital signal processing techniques, namely the space-time codes (Mumtaz *et al.* (2010)), from wireless communications are excellent candidates for mitigating PDL. In the case of Rayleigh fading in wireless communication systems, space-time codes are employed to create a dependence between the transmitted signals from each antenna such that even if there is a fading event and the SNR of any one channel reduces drastically, the data can be recovered successfully from the other channels. These space-time codes can be extended to polarization-time codes for PDM system with PDL. This improves the average performance of the system. The dependence of polarization-time codes as the name suggests is along both time and polarization dimensions.

Model of polarization dependent loss for a CO-OFDM system

Consider a PDM CO-OFDM system as described in Section (refer OFDM section) across two polarizations. A PDL channel can be modeled using a 2×2 matrix (similar to Jones Matrix). The OFDM system (after CP removal and FFT operations) can be written as (Shieh *et al.* (2007)),

$$\boldsymbol{Y}_{k,i} = \boldsymbol{H}_k\left(\omega_k\right)\boldsymbol{X}_{k,i} + \boldsymbol{N}_{k,i} \tag{2.21}$$

where $\boldsymbol{X}_{k,i}$ is the transmitted codeword (2×2) on the kth subcarrier on the ith OFDM symbol, $\boldsymbol{Y}_{k,i}$ is the corresponding received symbol, $\boldsymbol{H}_k\left(\omega_k\right)$ is the 2×2 frequency dependent PDL channel matrix and $\boldsymbol{N}_{k,i}$ is the additive noise component. Consider-

ing only PDL impairment, the channel matrix has the form (Desbruslais and Morkel (1994)),

$$\boldsymbol{H}_k\left(\omega_k\right) = \boldsymbol{H}_{PDL} = \boldsymbol{R}_\alpha \begin{bmatrix} \sqrt{1+\gamma_p} & 0 \\ 0 & \sqrt{1-\gamma_p} \end{bmatrix} \boldsymbol{R}_\alpha^{-1} \tag{2.22}$$

where $\boldsymbol{R}_\alpha$ ($\alpha \sim \text{Unif}[0, 2\pi)$) is a unitary random rotation matrix modeling the mismatch between the polarization axes of the transmitted signals and that of the polarization dependent element, $\gamma_p < 1$ quantifies the fluctuation in OSNR, $\Gamma_{dB} = 10\log_{10}\frac{1+\gamma_p}{1-\gamma_p}$ is the PDL coefficient in dB or simply the PDL. It is to be noted that in this model, the total energy between the two polarizations is constant regardless of the value of γ_p as any scaling can be absorbed into the covariance matrix of the noise vector. This formulation models the interaction of the two polarizations through redistribution of the power between them. In reality, due to the time varying nature of γ_p, the probability density function of PDL is a Maxwellian (Mecozzi and Shtaif (2002)). However, in this report, the PDL is assumed to be a constant. In the next section, the coding and decoding strategy of the Silver code, a popular family of space-time codes, are discussed. The Silver code is a very promising candidate for mitigating PDL induced performance degradation (Awwad *et al.* (2013)).

Coding and decoding

The transmitted symbols in a polarization-time coding scheme are dependent along both time and polarization dimensions. A 2×2 scheme is considered in this study. The transmitted signal can be expressed as a 2×2 codeword matrix across two consecutive time slots (T_1, T_2) and two polarizations (Pol_1, Pol_2).

$$\boldsymbol{X} = \begin{bmatrix} X_{Pol_1,T_1} & X_{Pol_1,T_2} \\ X_{Pol_2,T_1} & X_{Pol_2,T_2} \end{bmatrix}. \tag{2.23}$$

The codeword matrix of Silver code from four M-QAM symbols S_1, S_2, S_3, S_4 is:

$$\begin{aligned} \boldsymbol{X} &= \begin{bmatrix} S_1 + Z_3 & -S_2^* - Z_4^* \\ S_2 - Z_4 & S_1^* - Z_3^* \end{bmatrix} \\ \begin{bmatrix} Z_3 \\ Z_4 \end{bmatrix} &= \frac{1}{\sqrt{7}} \begin{bmatrix} 1+j & -1+2j \\ 1+2j & 1-j \end{bmatrix} \begin{bmatrix} S_3 \\ S_4 \end{bmatrix} \end{aligned} \tag{2.24}$$

Equation (2.24) clearly indicates that the coding scheme does not require any overhead and results in a full-rate transmission. The transformation from M-QAM symbols to codeword matrix is energy preserving. This means that the performance of this coded scheme in the absence of PDL ($\Gamma_{dB} = 0$) is identical to that of the AWGN performance of the uncoded scheme. There are 4^M codewords in the codebook $\mathscr{C}$. After this mapping, OFDM subcarriers of approriate polarization and time slots are filled with these codeword symbols. Figure 2.12 depicts the constellation diagram of the 256 complex codewords in the Silver code codeword space obtained from a unit power QPSK constellation using equation (2.24). The modulation process after this is as described in Section (refer to section 2.1).

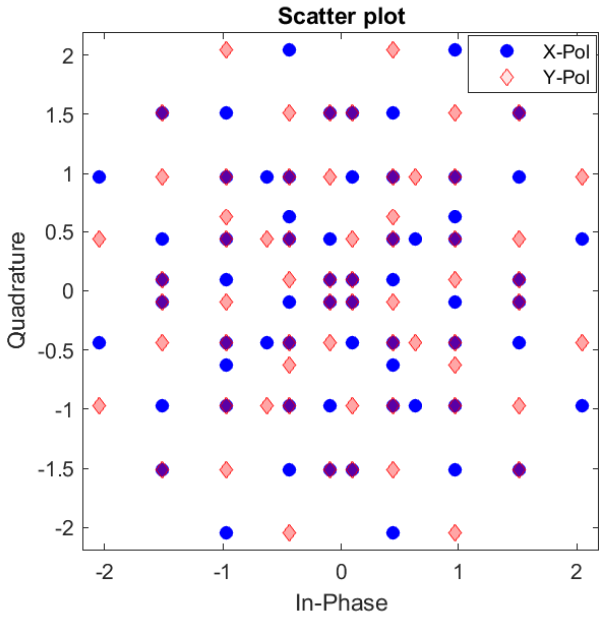

Figure 2.12: Constellation diagram of the codewords from Silver code from a power normalized QPSK constellation.

At the receiver, the received matrix in equation (2.21) is optimally decoded using the maximum likelihood (ML) decoding strategy. The decoder computes the estimate of the transmitted codeword according to,

$$\hat{\boldsymbol{X}} = \underset{\boldsymbol{X} \in \mathscr{C}}{\arg\min} ||\boldsymbol{Y} - \boldsymbol{H}\boldsymbol{X}||^2. \tag{2.25}$$

The decoding is performed as an exhaustive search over the codeword space $\mathscr{C}$ assuming a constant PDL channel matrix over the codeword duration. For 4-QAM

(QPSK) modulation, this exhaustive search is still practical. In a real system, the PDL matrix $\boldsymbol{H}$ has to be estimated periodically. This can be done using the preamble in each OFDM block. Apart from optimal ML decoding, there are other sub-optimal decoding techniques used for Silver codes. One of them is the sphere decoding technique (Damen *et al.* (2000)). In the next subsection, the performance of Silver codes generated from QPSK modulation format and decoded using the ML rule is studied through simulations.

Simulation results and discussion

A CO-OFDM system with PDL is simulated in MATLAB using the model (equations 2.21, 2.22), coding and decoding strategies (equations 2.24, 2.25) given in the above sections. The simulation setup considers PDL as the only impairment and assumes that the channel matrix is known to the receiver. Therefore, the length of cyclic prefix is set to zero. For a fixed Γ_{dB}, the rotation matrix $\boldsymbol{R}_{\alpha}$ is generated randomly for each OFDM block. The BER performance is the averaged performance for $\alpha \sim \text{Unif}[0, 2\pi)$.

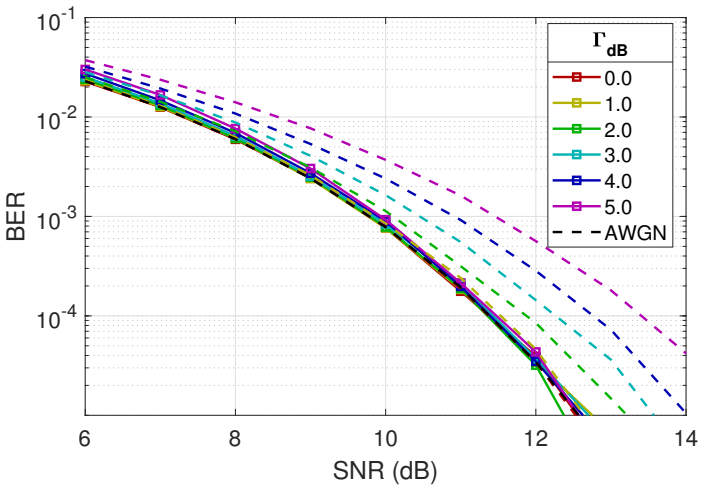

Figure 2.13: BER performance of Silver coded scheme (solid curves) and uncoded scheme (dashed curves) for different Γ_{dB}.

Figure 2.13 shows the error performance versus SNR for various PDL values (Γ_{dB}). For a fixed SNR, as Γ_{dB} increases, the performance of the uncoded scheme degrades, while that of the uncoded scheme is unchanged. As mentioned previously, the BER curve for the uncoded scheme for $\Gamma_{dB} = 0$ coincides with that of the coded scheme for $\Gamma_{dB} = 0$. Figure 2.14 renders the SNR penalty at BER $= 10^{-3}$ as a function of Γ_{dB}

for Silver coded and uncoded schemes. For $\Gamma_{dB} = 5$, the SNR penalty for uncoded scheme is more than $1.5\,dB$ but for the coded scheme it is just $0.1\,dB$. This shows the efficacy of the Silver code in mitigating PDL. The advantages of Silver codes in this context are zero-overhead, resilience to large PDL and ability to perform in conjugation with FEC. However, current systems use single carrier transmission and a decoder for silver codes would involve multitap modeling of the channel PDL matrix leading to large complexity at the receiver. Also, these codes assume that the PMD is negligible in the system or even if PMD exists, the cyclic prefix should be able to absorb it (Awwad *et al.* (2013)). Thus in a long haul link, the typical strategy is to leave a margin for PDL related SNR penalty and ensure that the PDL of each individual element is minimal.

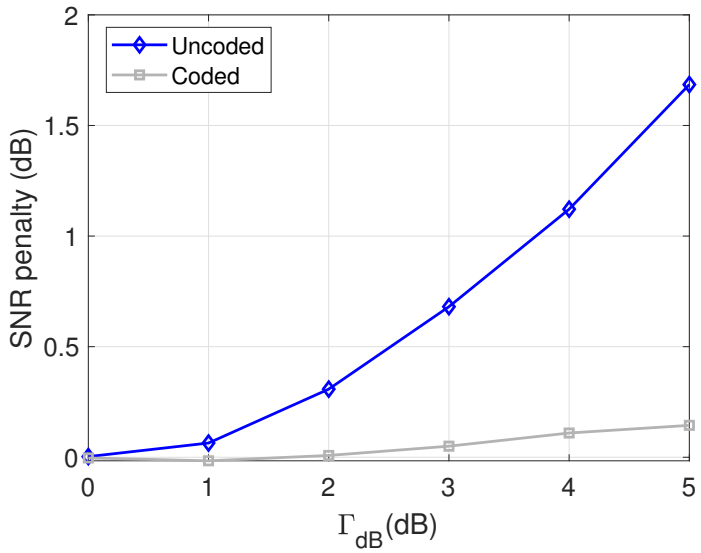

Figure 2.14: SNR penalty at BER $= 10^{-3}$ of Silver coded scheme (gray curve) and uncoded scheme (blue curve).

The extension of space-time codes to optical communication is not limited to PDM systems. The fading-like effect in mode division multiplexed systems due to mode mixing and mode dependent loss can also be mitigated by using these codes. For a note on this application see Appendix A.

2.2.4 Laser phase noise

While OFDM is resilient to linear impairments, due to its longer symbol duration and its frequency domain structure, it is more sensitive to laser phase noise (Wu and Bar-Ness (2004)). Lasers exhibit fluctuating optical phase and instantaneous oscillating fre-

quency (Schawlow and Townes (1958)). This leads to a non-zero laser linewidth. The laser phase noise on CO-OFDM systems is manifested as a Common Phase Error (CPE) and Inter Carrier Interference (ICI). The fluctuating phase of the laser is imprinted on the data and this nonlinear impairment breaks the orthogonality of the subcarriers. The average complex amplitude of this time varying impairment over an OFDM symbol contributes to the CPE and their higher frequency components cause interference between the subcarriers (ICI).

The time varying optical phase $\phi(t)$ of a laser due to non-zero linewidth can be modeled as a Wiener process (El-Tanany *et al.* (2001)).

$$\begin{aligned} \phi(t_2) &= \phi(t_1) + \Delta\phi; t_1 < t_2 \\ \Delta\phi &\sim \mathcal{N}\left(0, 2\pi\Delta\nu\left(t_2 - t_1\right)\right) \end{aligned} \tag{2.26}$$

where $\Delta\nu$ is the laser linewidth in Hz. In heterodyne coherent systems, this is the sum of the linewidths of transmitter and receiver lasers.

Thus over a symbol duration of T_s the average laser complex amplitude accumulates a random phase with variance $2\pi\Delta\nu T_s$. In the presence of laser phase noise and AWGN, the OFDM received symbols (after CP removal and FFT operation) can be expressed as (Wu and Bar-Ness (2004)),

$$Y_m(k) = X_m(k)I_m(0) + \text{ICI}_m(k) + N_m(k) \tag{2.27}$$

where $X_m(k)$ is the transmitted symbol in the kth subcarrier ($k = 0, 1, \ldots, N_{\text{FFT}}$) of the mth OFDM symbol, $N_m(k) \sim \mathcal{N}\left(0, \sigma^2\right)$ is the corresponding AWG noise term, $I_m(0)$ is the CPE factor and $\text{ICI}_m(k)$ are the ICI terms. Here the channel is assumed to be frequency flat. This is a valid assumption in a dispersion free optical fiber channel. The ICI terms are defined as (Wu and Bar-Ness (2004)),

$$\text{ICI}_m(k) = \sum_{l=0, l\neq k}^{N_{\text{FFT}}-1} X_m(l)I_m(l-k) \tag{2.28}$$

$$I_m(p) = \frac{1}{N_{\text{FFT}}} \sum_{n=0}^{N_{\text{FFT}}-1} e^{j\left[\frac{2\pi pn}{N_{\text{FFT}}} + \phi_m(n)\right]} \tag{2.29}$$

where $\phi_m(n), n = 0, 1, \ldots, N_{\text{FFT}} - 1$ is the sequence of time varying phase. In the case of zero linewidth, as $\phi_m(n)$ is a constant across time, $\text{ICI}_m(k) = 0$ and $|I_m(0)| = 1$.

Due to linewidth, the performance degradation is due to both the presence of ICI terms and due to reduction of signal power by the factor $|I_m(0)|^2 < 1$. This degradation can be quantified using the signal to interference plus noise (SINR) ratio. For low linewidths, the SINR is given as (Wu and Bar-Ness (2004)),

$$\Gamma = \frac{1 - \frac{\pi \Delta \nu T_s}{3}}{\frac{\pi \Delta \nu T_s}{3} + \frac{1}{\gamma_s}} \tag{2.30}$$

where $\gamma_s = E_s/\sigma^2$ is the SNR.

Mitigation of phase noise involves estimating and correcting for the CPE. For this, one can assume that the CPE term $I_m(0) \approx exp(j\theta(m))$, where θ_m is the common phase.

$$\theta(m) = \arg \left\{ \frac{1}{N_{\text{FFT}}} \sum_{n=0}^{N_{\text{FFT}}-1} e^{j\phi_m(n)} \right\} \tag{2.31}$$

$\theta(m)$ can be modeled as a Wiener process,

$$\Delta\theta(m) \triangleq \theta(m) - \theta(m-1) \sim \mathcal{N}\left(0, 2\pi.\Delta\nu T_s\right) \tag{2.32}$$

The CPE estimate $\hat{\theta}_m$ should be updated every symbol in order to successfully mitigate phase noise. CPE correction involves rotating the data in each subcarrier through $-\hat{\theta}_m$ radians.

$$\tilde{Y_m}(k) = Y_m(k)e^{-j\hat{\theta}_m}, k = 0, 1, \ldots, N_{\text{FFT}} - 1 \tag{2.33}$$

where $\tilde{Y_m}(k)$ is the CPE corrected received OFDM signal.

Equations (2.30) and (2.32) indicate that the quantity $\Delta\nu T_s$ captures the effect of phase noise. It is the combined contribution of the uncertainty in laser frequency (linewidth) and the duration of the OFDM symbol (T_s) over which the phase fluctuations accumulate. In the next section, a common technique for CPE estimation, the Pilot Aided technique (Yi *et al.* (2007)) is discussed.

Pilot aided technique

The pilot aided (PA) technique uses dedicated subcarriers for CPE estimation. These pilot subcarriers are interspersed among the data subcarriers and carry known data. The CPE estimate is obtained from the mean of the complex data in these pilot subcarriers at the receiver. The estimate $\hat{\theta}_m$ is given as,

$$\hat{\theta}_m = \arg\left\{\frac{1}{N_p}\sum_{l\in\mathscr{P}}\frac{Y_m(l)}{X_m(l)}\right\} \tag{2.34}$$

where N_p is the number of pilot subcarriers and $\mathscr{P}$ is the set of pilot subcarrier indices. Larger the value of N_p, better the estimate of CPE. However, increasing the number of pilot subcarriers will reduce the spectral efficiency.

Table 2.3: CO-OFDM parameters for simulation: Pilot Aided CPE estimation

Parameter	Value
Symbol Rate R_s	$32\,Gbaud$
Modulation	16 QAM
FFT size N_{FFT}	128
OFDM symbols N_{symb}	512
Filled Bandwidth	$25.6\,GHz$
PRBS order	15
Number of pilots N_p	12

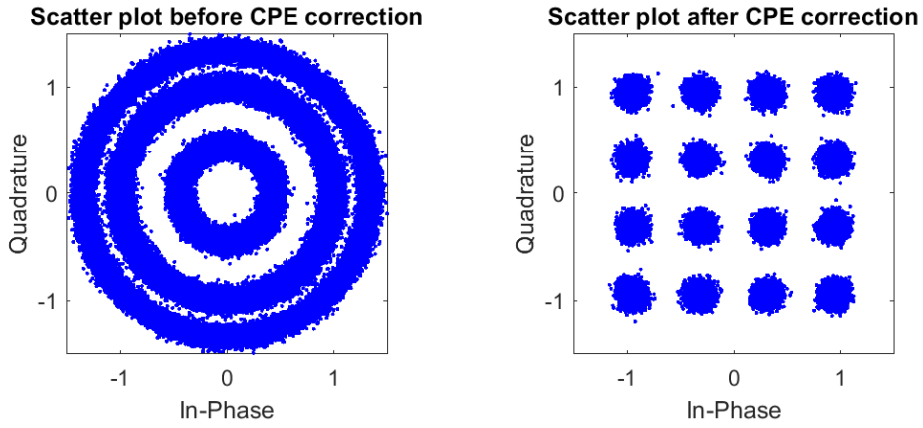

Figure 2.15: Constellation diagrams of a 16 QAM CO-OFDM signal before (left) and after (right) Pilot aided (PA) CPE estimation and correction. Note: the constellations have been normalized to unit power.

Simulations of a PM-16-QAM 32-GBd CO-OFDM signal with phase noise were run in MATLAB with the Optilux package. Table 2.3 contains the relevant simulation

parameters. Phase noise is generated according to equation (2.32). Figure 2.15 shows the constellation diagrams with and without CPE correction. To understand the effect of ICI, the error performance at different OSNR is also studied through simulations. Figure 2.16 renders the BER performance as a function of OSNR. The performance becomes poorer as the linewidth increases. This can be attributed to the increased power of ICI terms and subsequent degradation in SINR.

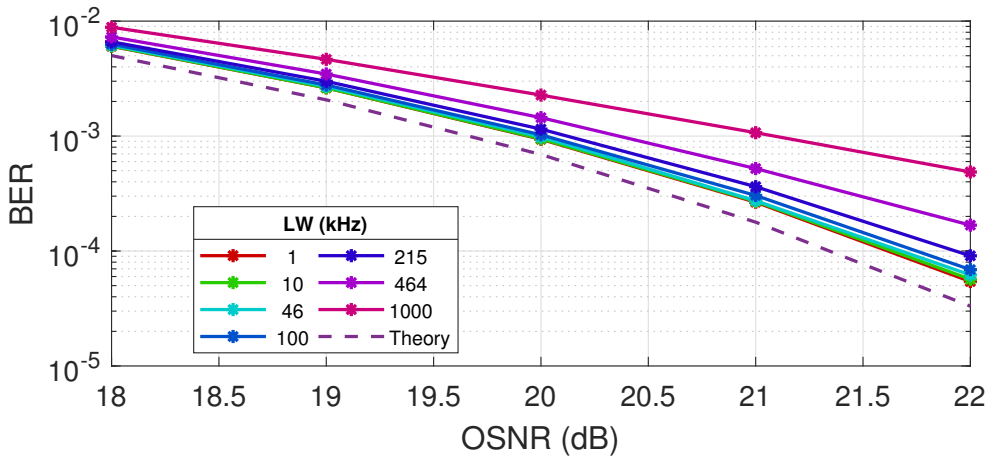

Figure 2.16: BER performance of pilot aided CPE estimation and correction for different laser linewidths.

Blind phase noise mitigation

Pilot aided phase noise mitigation techniques are effective but they require dedicated subcarriers, thereby reducing the throughput and spectral efficiency. Blind techniques have zero bandwidth overhead but may require more computations at the receiver. Some blind algorithms use decision directed iterative algorithms (Ha and Chung (2013),Mousa-Pasandi and Plant (2010)). These are prone to catastrophic failures in case of error propagation or poor initialization and are computationally expensive.

We propose a blind phase noise mitigation technique (K4P) which uses multilevel QPSK partitioning (Fatadin *et al.* (2014)) to estimate the CPE and Kalman filtering (Kálmán (1960)) to condition the estimates. The K4P technique can potentially work with any square M-QAM system. The innermost and the outermost points of a Square M-QAM constellation can be assumed to come from QPSK constellation but with different amplitude scaling. The fourth power rule (Viterbi (1983)) for carrier recovery in QPSK systems is used to estimate the phase angle.

Multilevel QPSK partitioning Let $\hat{\theta}_{m,o}$ and $\hat{\theta}_{m,i}$ be the estimates from the subcarriers carrying outer and inner constellation points respectively. The estimates from outer points will be more accurate as their SNR's would be better. Thus we generate a weighted average of $\hat{\theta}_{m,o}$ and $\hat{\theta}_{m,i}$, the estimates from the QPSK partitioning.

$$\hat{\theta}_{m,q} = \gamma_w \hat{\theta}_{m,o} + (1 - \gamma_w)\hat{\theta}_{m,i} \tag{2.35}$$

where the ratio of γ_w and $1 - \gamma_w$ is the ratio of the amplitudes of the outer and inner constellation points in the ideal case. Thus $\gamma_w = 0$ for QPSK, $\gamma_w = 0.75$ for 16 QAM and $\gamma_w = 0.875$ for 64 QAM. In order to avoid phase slips, the fourth power technique must be applied only after derotating the data in each subcarrier of the symbol by the CPE estimate from the previous symbol. The first symbol of the frame is assumed to be known and its CPE can be measured just like in the pilot aided case.

Kalman filter To generate a better estimate from $\hat{\theta}_{m,q}$, Kalman filter is used. Kalman filter is an estimation algorithm that uses a sequence of noisy observations and produces estimates of unknown variables. In its framework, there is a state equation and a measurement equation, both of which can be stochastic in nature. The state equation describes the evolution of state variables over time. The measurement equation describes the relation between the measured quantities and the current state variables. The measured quantities arrive sequentially and the state variables are estimated. Kalman filter is a recursive two step process, there is a prediction step and an update step. In the prediction step, the information on the current state is used to predict the next state and generate an estimate. In the update step, another estimate from a new measurement is generated and a weighted average of the two estimates according to their covariances (uncertainties) is reported as the final estimate for that iteration. The covariances are updated for the next prediction and update step.

In the case of blind CPE estimation, the process equation is the familiar Wiener process,

$$\theta(m) = \theta(m-1) + \Delta\theta(m) \tag{2.36}$$

where $\Delta\theta(m) \sim \mathcal{N}\left(0, 2\pi.\Delta\nu T_s\right)$ is the process noise and the measurement equation is,

$$\hat{\theta}_{m,q} = \theta(m) + \delta\theta(m) \tag{2.37}$$

where $\delta\theta(m) \sim \mathcal{N}\left(0, \sigma^2_{m,q}\right)$ is the measurement noise which depends on the OSNR of the signal and the number of subcarriers from which the estimate $\hat{\theta}_{m,q}$ was generated.

Table 2.4: CO-OFDM parameters for simulation: K4P blind CPE estimation

Parameter	Value
Symbol Rate R_s	$32\,Gbaud$
Modulation	16 QAM
FFT size N_{FFT}	128
OFDM symbols N_{symb}	512
Filled Bandwidth	$25.6\,GHz$
PRBS order	15

Simulation results A PM CO-OFDM system with phase is simulated in the back-to-back configuration in MATLAB. The relevant parameters are given in table 2.4. The detailed algorithm of the blind phase mitigation is given in Appendix B. Figure 2.17 shows the working of the two components of the K4P algorithm - the multilevel QPSK partitioning and the Kalman filter. The CPE estimate is taken as the average from both X and Y polarization components. This is assuming that the X and Y polarizations are aligned (perfect synchronization).

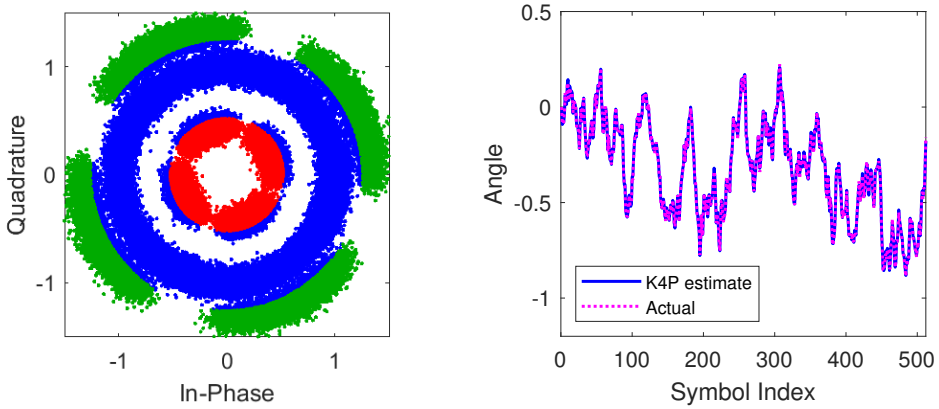

Figure 2.17: Working of K4P blind phase mitigation algorithm. The constellation diagram (left) shows the multilevel QPSK partitioning for a 16 QAM CO-OFDM system with phase noise. The inner points marked in red and the outer points in green. The phase tracking is done using Kalman filter (right). Note: the constellation has been normalized to unit power.

The efficacy of the algorithm is tested through these simulations and the bit error performance is plotted in figure 2.18. Similar to the PA case, the BER performance for higher combined laser linewidths is poorer. In order to compare the two schemes,

the OSNR penalty at BE$R = 10^{-3}$ is measured. Also, normalized linewidth $\Delta\nu T_s$ is taken as the argument as increasing the linewidth or increasing the symbol duration by the same factor are equivalent. Figure 2.19 shows the OSNR penalty variation for the pilot aided algorithm (for 8, 12 and 16 pilots) and for the K4P algorithm. The trends are similar: the penalty increases with the normalized linewidth. The performance of the blind algorithm is very comparable to that of the PA algorithm with 12-16 pilots. This means that in a long haul link, the pilots can be dropped and substituted with data subcarriers thereby increasing the throughput and spectral efficiency. In a multichannel system, these pilots can be dropped to reduce the channel overlap/crosstalk or the channel spacing can be reduced to increase the spectral efficiency.

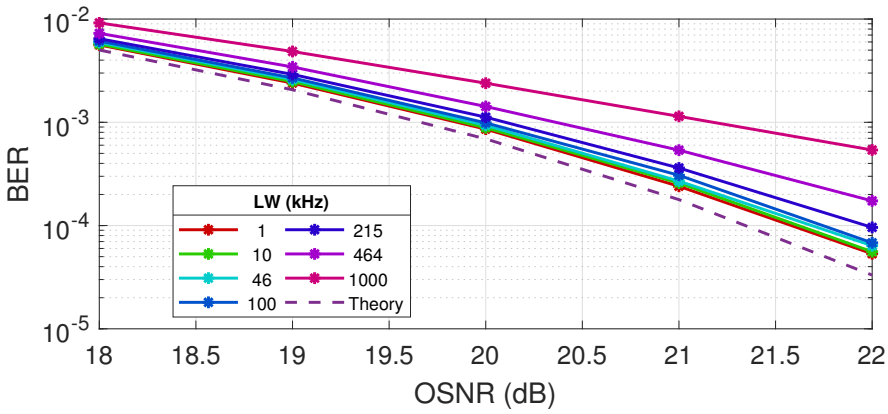

Figure 2.18: BER performance of blind K4P algorithm for CPE estimation and correction for different laser linewidths

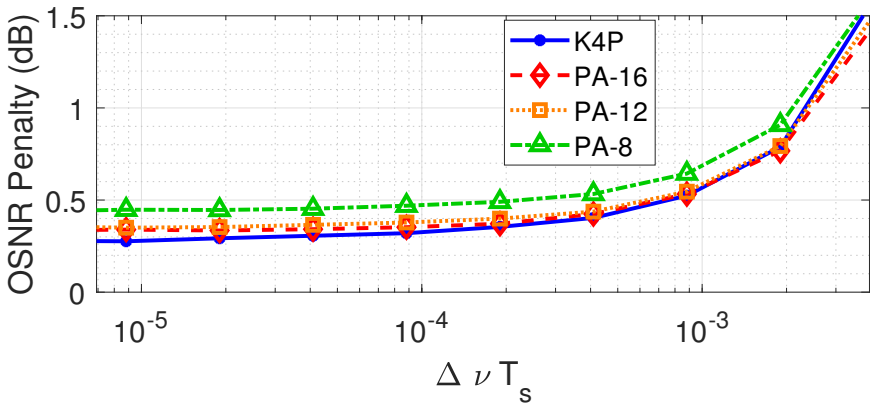

Figure 2.19: Performance comparison between blind phase noise algorithm and pilot aided algorithm. K4P denotes the blind algorithm and PA-N_p denotes the pilot aided algorithm employing N_p pilots

2.2.5 Hardware level impairments

Some common hardware level impairments in a CO-OFDM system are bandwidth limitations, IQ skew and modulator nonlinearity.

Bandwidth

The bandwidths of the transmitter and receiver limit the symbol rate (and the total available bandwidth). OFDM is designed to work in frequency-selective channels. If the channel state information is known to the transmitter, then it can boost the channels appropriately. A transmitter can have bandwidth limitations at the arbitrary waveform generator (AWG, the RF-OFDM source), the RF cables or at the optical modulator. Similarly the receiver may be limited by the bandwidths of the balanced photodiodes or the DAC. Each of these is a filter in series with the others. If the noise added by the channel is white in frequency, it becomes coloured by these filters. Channel equalization at the receiver ensures successful demodulation of the transmitted data, but the performance is limited by the SNR of the subcarriers. If the transmitter has bandwidth limitations, and the channel adds white noise, then SNR will be a function of the subcarrier channel response. A single polarization CO-OFDM system with transmitter side

Table 2.5: CO-OFDM parameters for simulation: Bandwidth

Parameter	Value
Symbol Rate R_s	$20\,Gbaud$
Modulation	QPSK
FFT size N_{FFT}	128
OFDM symbols N_{symb}	8192
Filled Bandwidth	$16\,GHz$
Number of pilots N_p	0
Length of cyclic prefix L_{CP}	8
OSNR	$15\,dB$

bandwidth limitations is simulated in MATLAB. The relevant simulation parameters are listed in table 2.5. A Bessel filter of order 5 with different bandwidths are used to filter the signal before adding white Gaussian noise. At the receiver the channel is equalized using a single tap equalizer for each subcarrier. The bandwidth is normalized to the symbol rate. The channel estimate is obtained by assuming that the first 10 transmitted

symbols are known to the receiver and averaging the individual estimates.

Figure 2.20 shows the channel estimate and subcarrier EVM plot for different normalized bandwidths for $15\,dB$ OSNR. The channel estimate and subcarrier EVM plots have an inverse dependence. A higher channel estimate means the SNR is high and the EVM is low. Figure 2.20 plots the EVM as a function of normalized bandwidth for $15\,dB$ OSNR and the BER variation with OSNR for different normalized bandwidths. The EVM reduces as the bandwidth increases because the number of subcarriers with higher SNR increases. Beyond normalized bandwidth of 1, the performance matches with theory. This indicates that the baudrate of the system should be well within the transmitter bandwidth.

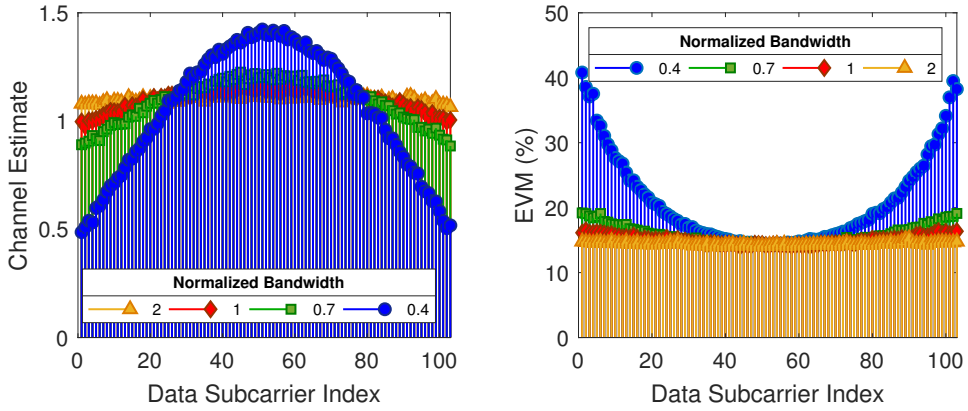

Figure 2.20: The channel estimate (left) and EVM (right) for each subcarrier for different normalized bandwidths for $15\,dB$ OSNR.

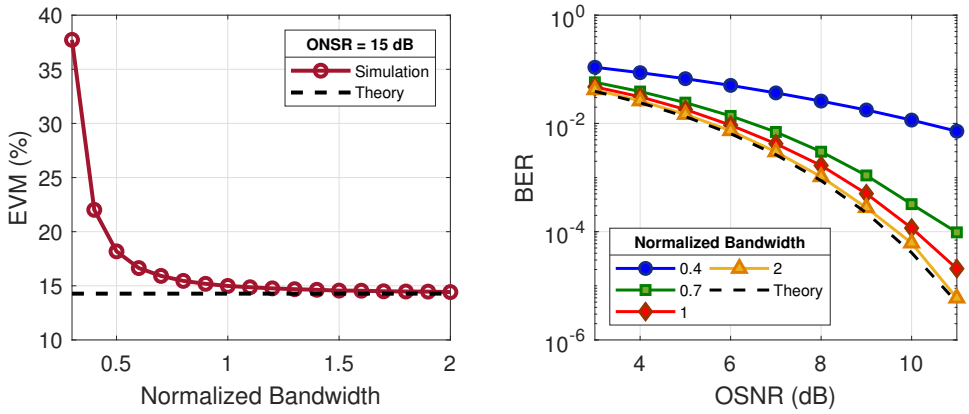

Figure 2.21: Effect of transmitter bandwidth on the EVM and BER performance. (Left) The dashed line denotes the ideal EVM for OSNR of $15\,dB$. (Right) The dashed line denotes the ideal BER curve in AWGN channel.

If the channel estimates are available to the transmitter, then pre-compensation of

the signal can be done to ensure uniform EVM performance. Pre-compensation involves transmitting X_k/H_k on the kth subcarrier, thereby, strengthening weak channels. The transmit power, however is kept constant. Figure 2.22 shows the channel estimates and EVM as a function of the subcarrier for different normalized bandwidths. The channel estimates from the previous exercise is fed into the OFDM signal generation module for a point-by-point division with the signal in each subcarrier. The EVM and channel estimate has become uniform across the subcarriers indicating successful pre-compensation. The EVM is higher for lower normalized bandwidths because of higher loss of signal power due to the filtering at lower bandwidths and subsequent reduction in SNR.

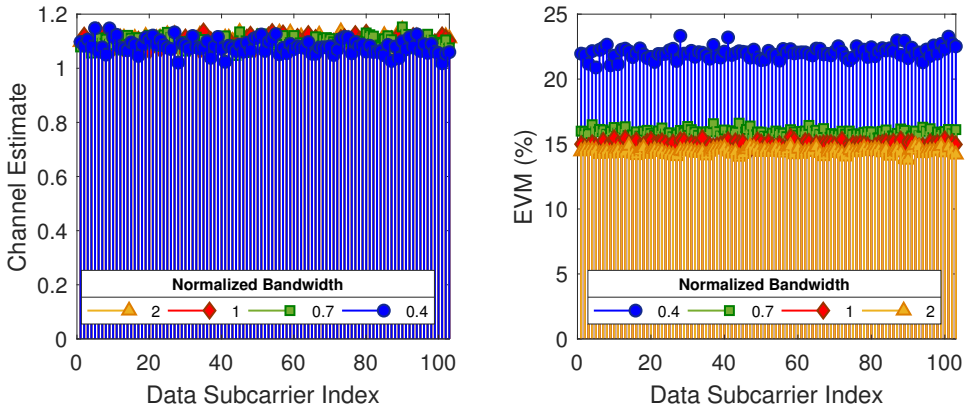

Figure 2.22: The channel estimate (left) and EVM (right) for each subcarrier for different normalized bandwidths after pre-compensation for $15\,dB$ OSNR.

IQ Skew

IQ skew is the synchronization delay between the I and Q channels of the hardware at the transmitter or receiver. It is a nonlinear impairment that causes ICI. IQ skew could be due to many reasons - mismatch in RF cable lengths and phase response of filters of I and Q channels giving different group delays are a few. Consider a signal $x(t) = x_r(t) + jx_i(t)$ and its continuous time Fourier transform $X(j\omega)$,where $x_r(t)$ and $x_i(t)$ are real. Denote the Fourier transforms of $x_r(t)$ and $x_i(t)$ as $X_r(j\omega)$ and $X_i(j\omega)$.

$$\begin{aligned} X_r(j\omega) &= \frac{1}{2}\left\{X(j\omega) + X^*(-j\omega)\right\} \\ X_i(j\omega) &= \frac{1}{2j}\left\{X(j\omega) - X^*(-j\omega)\right\} \end{aligned} \tag{2.38}$$

where $(^*)$ denotes conjugation operation.

For an IQ skew of $\Delta\tau_{IQ}$ units, the signal and its transform become,

$$x_{IQ}(t) = x_r(t) + jx_i\left(t - \Delta\tau_{IQ}\right) \tag{2.39}$$

$$\begin{aligned} X_{IQ}(j\omega) &= X_r(j\omega) + jX_i(j\omega)e^{-j\omega\Delta\tau_{IQ}} \\ &= \frac{1}{2}\left\{X(j\omega) + X^*(-j\omega)\right\} + \frac{1}{2}\left\{X(j\omega) - X^*(-j\omega)\right\}e^{-j\omega\Delta\tau_{IQ}} \\ &= X(j\omega)\left\{\frac{1}{2} + \frac{1}{2}e^{-j\omega\Delta\tau_{IQ}}\right\} + X^*(-j\omega)\left\{\frac{1}{2} - \frac{1}{2}e^{-j\omega\Delta\tau_{IQ}}\right\}. \end{aligned} \tag{2.40}$$

We see that $X_{IQ}(j\omega)$ simplifies to $X(j\omega)$ when $\Delta\tau_{IQ} = 0$. For nonzero $\Delta\tau_{IQ}$, there is interference from the $X(-j\omega)$ component. In the case of a complex OFDM signal, this would correspond to the mirror subcarrier which would carry independent data and this interference would be random. The subcarrier of index $k, k = 0, 1, 2, \ldots N_{\text{FFT}} - 1$ faces interference from the subcarrier of index $N_{\text{FFT}} - k$. The DC subcarrier does not face any interference. Not only does the skew induce an interference, the signal amplitude is also reduced by the factor $(1 + e^{-j\omega\Delta\tau_{IQ}})/2$. The signal to interference ratio (SIR) is a function of the subcarrier frequency and can be written as,

$$\begin{aligned} \text{SIR}(\omega) &= \left|\frac{1 + e^{-j\omega\Delta\tau_{IQ}}}{1 - e^{-j\omega\Delta\tau_{IQ}}}\right|^2 \\ &= \frac{1 + \cos(\omega\Delta\tau_{IQ})}{1 - \cos(\omega\Delta\tau_{IQ}}) \\ &\approx \frac{1}{\sin^2(\omega\Delta\tau_{IQ}/2)} \\ &\approx \frac{4}{\omega^2\Delta\tau_{IQ}^2} \end{aligned} \tag{2.41}$$

where the approximations are for $\omega\Delta\tau_{IQ} \ll 1$. The SIR of the subcarrier decreases quadratically with the subcarrier frequency. Therefore EVM $\propto 1/\sqrt{\text{SIR}}$ increases linearly with the subcarrier frequency. The EVM of a specific subcarrier also increases linearly with the IQ skew. This IQ skew can be at the transmitter or the receiver.

The effect of IQ skew is simulated for a single polarization OFDM system in MATLAB. The channel is assumed to be flat and noiseless. Only the effect of IQ skew is simulated for the typical IQ skew values in practice ($\sim 1\,ps$). The relevant parameters

Table 2.6: CO-OFDM parameters for simulation: IQ skew

Parameter	Value
Symbol Rate R_s	$20\,Gbaud$
Modulation	QPSK
FFT size N_{FFT}	128
OFDM symbols N_{symb}	512
Filled Bandwidth	$16\,GHz$
Number of pilots N_p	0
Length of cyclic prefix L_{CP}	0
PRBS order	15

are listed in table 2.6. The EVM of each subcarrier is depicted graphically in figure 2.23. V-shaped EVM curves are obtained. The EVM for the outermost subcarrier in figure 2.23 for $\Delta\tau_{IQ} = 2\,ps$ is about 7% and for $\Delta\tau_{IQ} = 1\,ps$ is about 3.5%. These are consistent with the above analysis that the subcarriers at higher frequency face stronger interference and the strength of the interference increases quadratically giving a linear relationship between EVM and subcarrier frequency, and EVM and IQ skew.

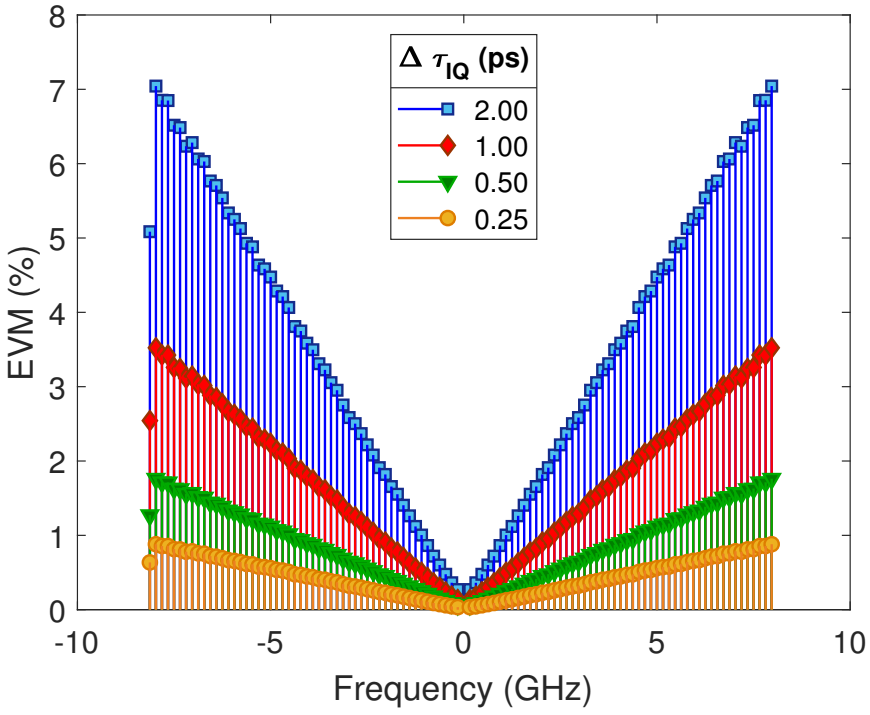

Figure 2.23: EVM performance per subcarrier for different IQ skew values. The signal band is partially filled, $16\,GHz$ out of $20\,GHz$.

The OFDM symbol period of this simulation is $6.4\,ns$ and the IQ skew considered in the simulations are three orders smaller than this and yet, the EVM degradation can

be as high as 7%. For a QPSK-OFDM system, this corresponds to 23 dB SIR thereby limiting the system performance. In a practical implementation, IQ skew can be made limited by ensuring symmetry in I and Q channels and any residual IQ skew can be measured using a high sampling rate real time scope and corrected digitally.

Modulator Nonlinearity

Electro-optic modulators are used for upconversion of baseband signal to the optical frequency. The nonlinearity in these modulators is due to their cosine transfer function. Shieh *et al.* (2008) present the two-tone intermodulation analysis to quantify the non-linear effect. Two complex tones at $v_1 = ve^{j\omega_1 t}$ and $v_1 = ve^{j\omega_2 t}$ are applied to the input of the optical IQ modulator. The output of the modulator is,

$$E(t) = A\text{cos}\left(\frac{\pi}{2}\frac{V_I + V_{DC}}{V_\pi}\right)e^{j\{\omega_0 t+\phi_0\}} + A\text{cos}\left(\frac{\pi}{2}\frac{V_Q + V_{DC}}{V_\pi}\right)e^{j\{\omega_0 t+\phi_0+\pi/2\}} \quad (2.42)$$

where A is a proportionality constant, $V_I = v(\text{cos}\omega_1 t + \text{cos}\omega_2 t)$ and $V_Q = v(\text{sin}\omega_1 t + \text{sin}\omega_2 t)$ are the real and imaginary parts of complex RF input signal, V_{DC} is the applied DC bias, V_π is the half-wave switching voltage, ω_0 and ϕ_0 are the frequency and phase of the transmitter laser. The equivalent baseband transmitted signal from the modulator becomes (dropping the proportionality constant A),

$$E^B(t) = \text{cos}\left[\frac{M}{2}(\text{cos}\omega_1 t + \text{cos}\omega_2 t) + \frac{\phi}{2}\right] + j\text{cos}\left[\frac{M}{2}(\text{sin}\omega_1 t + \text{sin}\omega_2 t) + \frac{\phi}{2}\right] \quad (2.43)$$

where $M = \pi v/V_\pi$ is the modulation index, $\phi = V_{DC}\pi/V_\pi$ is the static phase shift (bias). Equation (2.43) can be expanded using Bessel functions and the fundamental output component with frequency $\omega_{1,2}$ is (Tang *et al.* (2007)),

$$E^B_{\omega_{1,2}}(t) = 2\text{sin}(\phi/2)J_0(M/2)J_1(M/2)e^{j\omega_{1,2}t} \quad (2.44)$$

where $J_n()$ is the Bessel function of the first kind with order n. Similarly, the second order intermodulation product at frequency $\omega_{1,2} - \omega_{2,1}$ can be expressed,

$$E^B_{\omega_{1,2}-\omega_{2,1}}(t) = 2\text{cos}(\phi/2)J_1^2(M/2)e^{j(\omega_{1,2}-\omega_{2,1})t} \quad (2.45)$$

and the third order products at frequency $2\omega_{1,2} - \omega_{2,1}$ as,

$$E^{B}_{2\omega_{1,2}-\omega_{2,1}}(t) = 2\text{sin}(\phi/2)J_1(M/2)J_2(M/2)e^{j(2\omega_{1,2}-\omega_{2,1})t}. \tag{2.46}$$

To characterize the modulator nonlinearity, intercept points are defined (Kolner and Dolfi (1987)). The second and third order intercept points are the points of intersection of the linear extension of second and third order intermodulation output powers with the linear extension of the fundamental output power. The intercept points are given in terms of the fundamental power.

$$IP2 = 2\text{sin}^4(\phi/2)/\text{cos}^2\phi/2 \tag{2.47}$$

$$IP3 = 4\text{sin}^2(\phi/2) \tag{2.48}$$

and the corresponding modulation indices,

$$M_{IP2} = 2\text{tan}(\phi/2) \tag{2.49}$$

$$M_{IP3} = 4\sqrt{2}. \tag{2.50}$$

Figure 2.24 renders the plots showing the powers of the fundamental component and the second and third order intermodulation products. By biasing at π we see that the second order products vanish and the nonlinearity is minimum. Thus the optimal bias point corresponds to the null bias. This is true for any modulation including OFDM. In OFDM, any pair of subcarriers will produce second and third order intermodulation products which will fall within the signal band and cause interference. The modulation index is related to the peak power of the signal and due to high PAPR, the modulation index for OFDM will be higher than single carrier signals with the same average power. As OFDM is more susceptible to nonlinearity, the swing voltage at the modulator input should be kept low. The bias should be fixed and controlled at $\phi = \pi$ point through active feedback techniques.

A CO-OFDM system with the parameters in table 2.5 is simulated. The modulation index $\pi v_{\text{peak}}/V_\pi$ is varied from $-20\,dB$ to $20\,dB$ and the EVM performance is obtained. Figure 2.25 shows the EVM and BER performance for different modulation indices. For low modulation index (or RMS voltage), the modulator operated in the linear regime

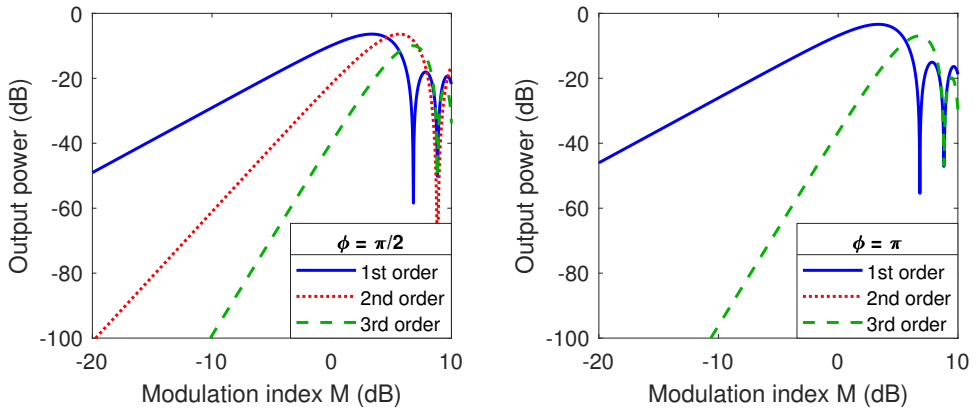

Figure 2.24: Effect of modulation index on fundamental, second and third order components of output power for bias $\phi = \pi/2$ (left) and $\phi = \pi$ (right).

and the performance is the same (minimum EVM limited to about 0.3% by simulation due to filtering, ideally it should be 0). As the modulation index of the input increases beyond $5\,dBm$, the nonlinearity starts degrading the performance, and beyond $0\,dB$ it is no longer of transmission quality. The operating point can be fixed between $-5\,dB$ and $0\,dB$. In the BER curves, there is close agreement with the theoretical curve upto $0\,dB$ modulation index. For $6\,dBm$, the BER starts to deviate from theory after $10\,dB$ OSNR and for higher modulation indices, the deviation occurs at even lower OSNR's indicating the dominance of nonlinear distortion over additive noise.

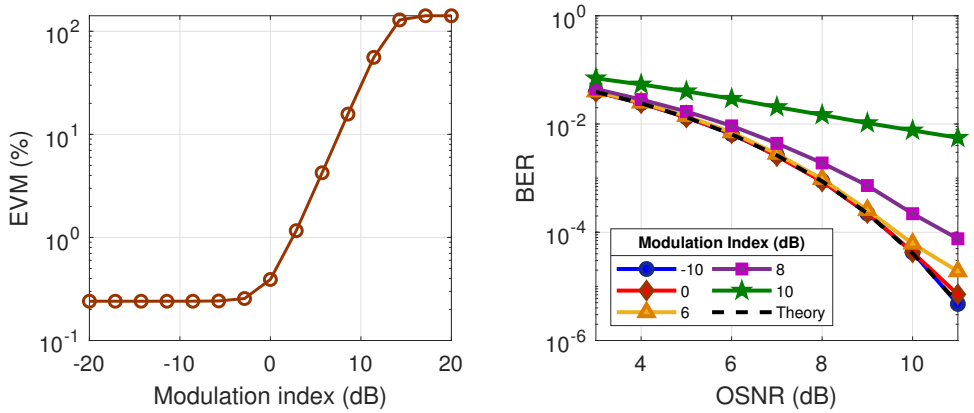

Figure 2.25: Effect of modulation index on the EVM and BER performance. (Left) The figure shows EVM for different modulation indices in the ideal no-noise case. (Right) The BER perforamnce for different modulation indices. The dashed line denotes the ideal BER curve in AWGN channel.

These hardware level impairments cannot always be handled digitally and hence impose strict limitations on signal parameters like bandwidth and launch power. The

system bandwidth ultimately limits the signal bandwidth. In the optical communication laboratory at IITM, the bandwidth of the system to $23\,GHz$ is limited by the AWG at the transmitter after which there is a roll-off. For a $32\,GBaud$ system, this corresponds to a filter of 0.72 normalized bandwidth and for a $21\,GBaud$ system, this corresponds to a filter of 1.1 normalized bandwidth. These systems are simulated in MATLAB for a combined linewidth of $100\,kHz$. The relevant parameters are listed in table 2.7. The entire bandwidth is filled save for the DC subcarrier. At the receiver, channel equalization, and CPE estimation and correction for phase noise are done. The BER performance for the systems are plotted in figure 2.26. The OSNR penalty at 10^{-3} BER is obtained as $4\,dB$ for the $32\,Gbaud$ system and $1.8\,dB$ for the $21\,Gbaud$ system respectively.

Table 2.7: CO-OFDM parameters for simulation: Analysis of Lab system

Parameter	Value
Symbol Rate R_s	$32\,Gbaud$/$21\,Gbaud$
Modulation	QPSK
FFT size N_{FFT}	128
OFDM symbols N_{symb}	512
Filled Bandwidth	$31.75\,GHz$/$20.8\,GHz$
Number of pilots N_p	8
Length of cyclic prefix L_{CP}	8
Combined Linewidth	$100\,kHz$
Bandwidth of transmitter	$23\,GHz$
IQ Skew	$1\,ps$

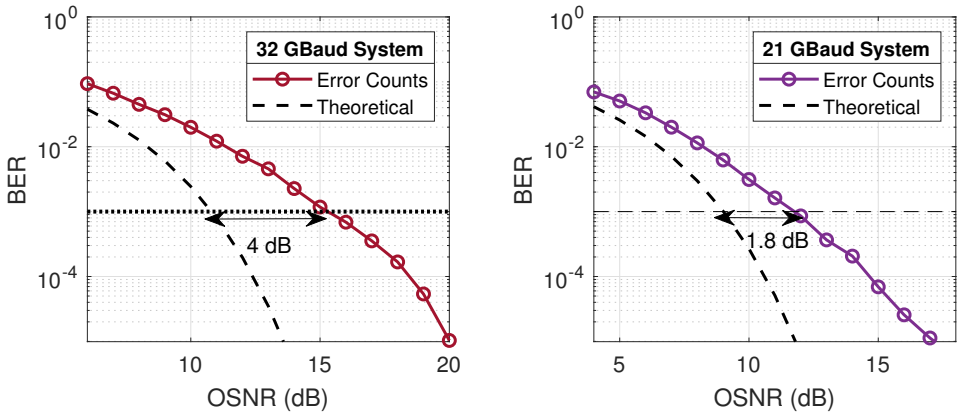

Figure 2.26: BER performance for the systems in table 2.7. (Left) for $32\,GBaud$ system and (right) for $21\,GBaud$ system. The dashed curves correspond to the ideal performance and the dotted line marks 10^{-3} BER.

Of the hardware impairments considered in this section, bandwidth is what ulti-

mately limits the data-rate and performance. The IQ skew in the order of $1\,ps$ limits the OSNR at the transmitter but this can be corrected after characterizing the system.

In this chapter, the common impairments in a CO-OFDM were considered. The high spectral efficiency of OFDM motivates us to study the suitability of CO-OFDM for long haul communication. The sensitivity of OFDM to nonlinearity makes fiber nonlinearity mitigation an important task for achieving longer reach and higher bit-rates. Digital compensation techniques like digital back propagation, however, are very computationally expensive, especially for systems like OFDM where the accuracy of compensation is critical. The computational burden would add on top of the $N_{\text{FFT}}\log_{10}\{N_{\text{FFT}}\}$ operations required for FFT/IFFT. As a result, all-optical techniques to mitigate nonlinearity and chromatic dispersion are promising alternatives. In the next chapter, an all-optical mid-span spectral inversion scheme for CO-OFDM systems using optical phase conjugation in SOA is presented.

CHAPTER 3

MID-SPAN SPECTRAL INVERSION FOR CO-OFDM USING SEMICONDUCTOR OPTICAL AMPLIFIERS

The increase in demand for better internet connectivity and data rates has necessitated the increase in the throughput of the long haul optical fiber channels (Cisco (2019)). But due to intrinsic nonlinear properties of optical fiber, the optical powers are constrained to be low. Low optical powers limit the OSNR values achievable after large propagation distances thereby limiting the use of advanced modulation formats to increase the throughput. Fiber Kerr nonlinearity ultimately limits the data rate of reliable transmission in these long haul links (Essiambre *et al.* (2008)). It is therefore important to mitigate nonlinearity to achieve high spectral efficiency (Ellis *et al.* (2010)).

There are several reports of improvement in performance after using nonlinearity mitigation techniques like digital back propagation (DBP) (Ip and Kahn (2008)). However, the high computational complexity of DBP makes it impractical in a link using multiple wavelength bands. This motivates the use of all optical methods that reduce the burden on DSP at the receiver.

Mid span spectral inversion (MSSI) uses optical phase conjugation (OPC) at the centre of the link and has the potential to compensate nonlinearity for multiple WDM channels (Morshed *et al.* (2013)). After nonlinearity was identified as important factor in the nonlinear Shannon limit (Essiambre *et al.* (2008)), MSSI seems to be a promising solution. MSSI is a nonlinear operation and third order (Kerr) nonlinear media ($\chi^{(3)}$ media) which exhibit four-wave mixing are suitable to realize this spectral inversion.

For CO-OFDM systems, MSSI has been reported both in simulations (Liu *et al.* (2010)) and experimental demonstrations (Du *et al.* (2012)). However the nonlinear medium of choice has been HNLF. In this report, the simulation performance of nonlinear semiconductor optical amplifier (SOA) as the medium for MSSI is studied. In the next section, the main reason why MSSI works is discussed.

3.1 Ideal MSSI for CO-OFDM

The nonlinear Schrodinger equation (NLSE) (equation 2.9) in the absence of attenuation can be written as,

$$\frac{\partial A(T,z)}{\partial z} + j\frac{\beta_2}{2}\frac{\partial^2 A(T,z)}{\partial T^2} - j\gamma|A(T,z)|^2 A(T,z) = 0 \tag{3.1}$$

where $A(T,z)$ is the envelope of the electric field. Taking the conjugate of this equation,

$$-\frac{\partial A^*(T,z)}{\partial z} + j\frac{\beta_2}{2}\frac{\partial^2 A^*(T,z)}{\partial T^2} - j\gamma|A^*(T,z)|^2 A^*(T,z) = 0 \tag{3.2}$$

where * denotes the conjugation operation. This describes the back-propagation of the signal through the fiber. If this conjugation is performed mid-span, it will result in nonlinearity and dispersion free output at the second half of the link. Intuitively the nonlinear and dispersive phase collected over the first half of the transmission link is conjugated and cancels the nonlinear and dispersive phase collected over the second half.

The above analysis neglected the attenuation term in the NLSE. For an ideal distortion free signal, if the first half has distributed loss due to attenuation, then the second half should have distributed gain. This is not practically possible. Furthermore, the dispersion parameters are not constant across the entire length of transmission. They fluctuate due to environmental and material non-uniformity (Watanabe and Shirasaki (1996)). Thus if MSSI is done exactly at the centre, there will be residual distortions. The OPC module need not be placed midway (Lorattanasane and Kikuchi (1997)). In this report, the study is limited to OPC at mid-span and the performance of SOA as a nonlinear medium for MSSI for CO-OFDM.

Simulation of ideal MSSI for CO-OFDM system

An ideal MSSI where the output complex electric field envelope is the conjugate of the input is simulated for an single polarization CO-OFDM system. $E_{\text{out}}(t) = E^*_{\text{in}}(t)$. The schematic of the system is shown in figure 3.1. An fiber optic link with N_{spans} spans of 80 km uncompensated SSMF fiber is considered. After each span, an amplifier (with noise figure 5 dB) compensates for the attenuation in the optical power. At the

Table 3.1: CO-OFDM parameters for simulation: Ideal MSSI

Parameter	Value	Parameter	Value
Symbol Rate R_s	$20\,Gbaud$	Signal Launch Power	$3\,dBm$
Modulation	QPSK/16 QAM	Length of Span	$80\,km$
FFT size N_{FFT}	128	EDFA Gain	$16\,dB$
OFDM symbols N_{symb}	128	EDFA Noise Figure	$5\,dB$
Filled Bandwidth	$16\,GHz$	Dispersion D	$17\,ps/nm.km$
Number of Pilots N_p	8	Nonlinearity γ	$2\,W^{-1}/km$
PRBS order	13	Attenuation α	$0.2\,dB/km$

mid-span, an ideal spectral inversion module is present. The relevant parameters are given in table 3.1. The input OSNR was set at $30\,dB$ and the optical launch power at $3\,dBm$ and the combined laser linewidth at $100\,kHz$. At the receiver, phase noise compensation using the pilot aided technique is done. There is no digital chromatic dispersion and nonlinearity compensation at the receiver.

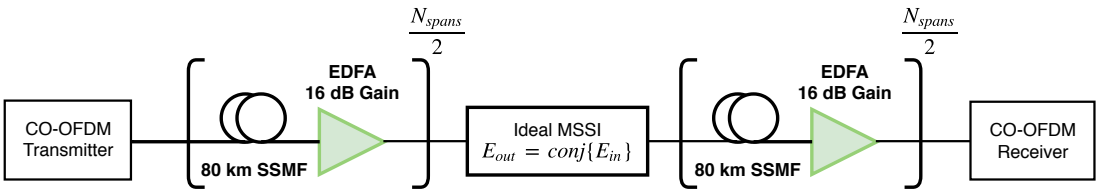

Figure 3.1: Schematic of Ideal MSSI for CO-OFDM. EDFA - Erbium Doped Fiber Amplifier, SSMF - Standard Single Mode Fiber, N_{spans} - Number of spans.

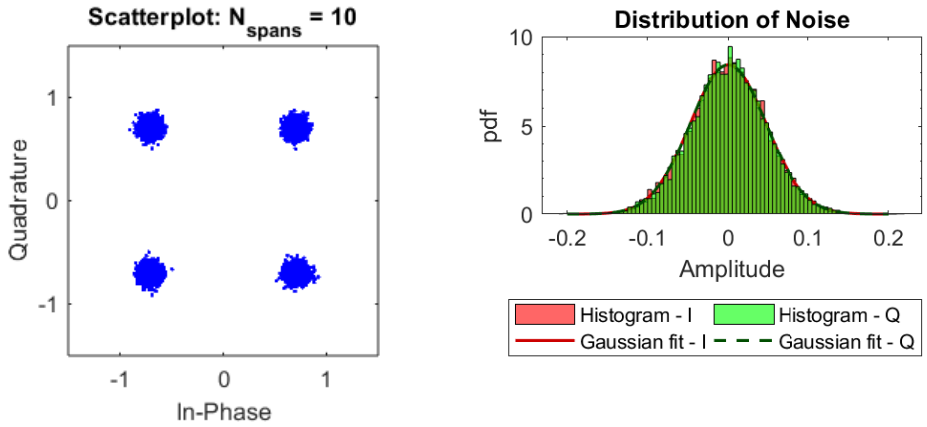

Figure 3.2: Simulation of Ideal MSSI: Constellation diagram (left) and histogram of noise (right) for a system with 10 spans. The EVM obtained is 6.7%.

Error vector magnitude (EVM) is taken as the metric of performance for three reasons. One, the BER through error counts was consistently zero for the range of oper-

ation considered. Two, the noise about the constellation points were almost Gaussian and EVM is a sufficient measure for Gaussian distribution (see figure 3.2). Three, EVM is independent of the modulation format.

The EVM performance for different number of spans (N_{spans}) was studied for the simulation parameters in table 3.1. The EVM result for both QPSK-CO-OFDM and 16 QAM-CO-OFDM systems are rendered in figure 3.3. The corresponding BER for MSSI case through error counts was zero. The increasing trend for the EVM is due to degrading OSNR and increasing residual nonlinear distortion with increasing number of spans. This result will serve as a reference for studying the performance of MSSI using SOA. It should be noted that the EVM performance of both QPSK and 16 QAM cases are the same. This is expected as EVM is independent of the modulation used. However, the BER for a given EVM is different for different modulation formats (equations 2.7,2.8, table 2.1).

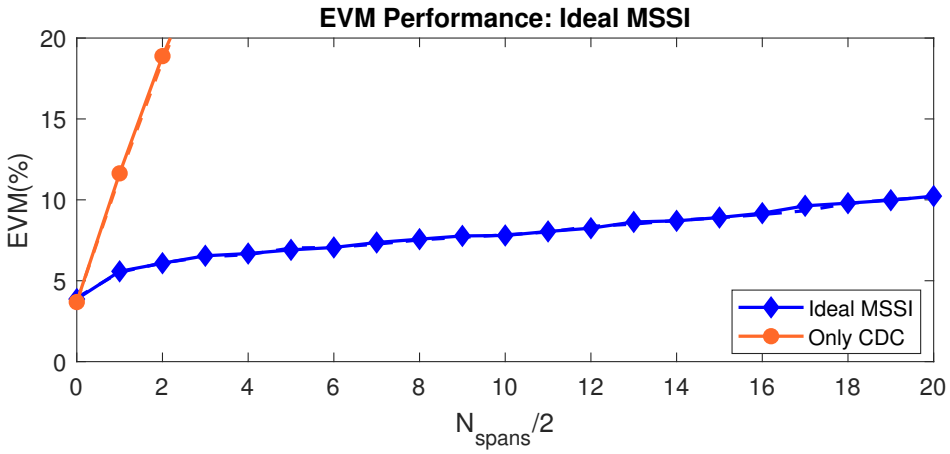

Figure 3.3: Effect of transmission distance on the EVM performance of Ideal MSSI; Signal launch power is $3\,dBm$. CDC - Chromatic dispersion compensation. Solid lines correspond to QPSK and dashed lines correspond to 16 QAM.

Figure 3.3 also shows the EVM curve for the case without MSSI for nonlinearity and chromatic dispersion mitigation. In this case, CD compensation is performed digitally using FDE. The figure clearly demonstrates the need for nonlinearity mitigation and the capability of MSSI for the same. As the launch power increases, the nonlinear effects increase in strength. Thus, the effect of signal launch power on the performance for a fixed transmission length of 10 spans is also studied. The signal power is varied from $-4\,dBm$ to $8\,dBm$. The EVM performance is plotted in figure 3.4. The EVM improves and later degrades with increasing signal power - from the ASE noise limited regime to

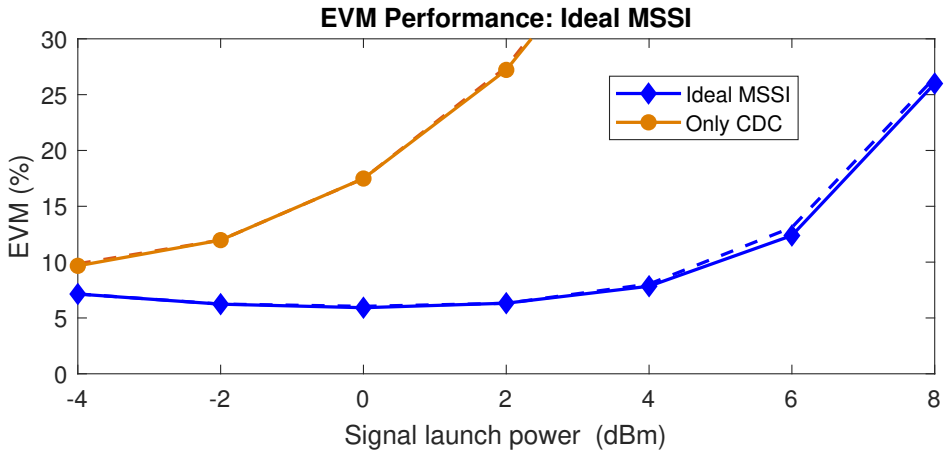

Figure 3.4: Effect of signal launch power on the EVM performance of Ideal MSSI; The transmission length is 800 km (10 spans). CDC - Chromatic dispersion compensation. Solid lines correspond to QPSK and dashed lines correspond to 16 QAM.

nonlinearity limited regime. The resilience of the MSSI scheme is seen from its EVM curve - the EVM performance starts to increase rapidly only after $4\,dBm$ launch power. On the other hand, for the non-MSSI case, it starts to increase from $-4\,dBm$ or lower power levels.

3.2 MSSI using semiconductor optical amplifier

Nonlinear semiconductor optical amplifiers (SOA) have become promising components for optical signal processing for communication applications. This is attributed to its small footprint, high nonlinearity, low pump power requirements and tolerable polarization sensitivity of less than 2 dB (Doussiere *et al.* (1995)). The nonlinearity in SOA is due to multiple mechanisms, one of which is four wave mixing (FWM) (Agrawal (1988)). When two co-polarized optical waves, a pump and a signal wave, at different frequencies are injected into the SOA the beating of both the waves produces dynamic gain and index gratings by modulating the carrier density and distribution in the active medium. These gratings produce new frequency components when a new wave interacts with them. The interband and intraband effects of SOA give rise to this FWM effect (Diez *et al.* (1997)). Interband interactions refer to the transitions between the valence and the conduction band and intraband interactions refer to the modulation of the distribution within the bands. Carrier density pulsation (CDP) is an interband effect

that changes the carrier density through simulated emission and subsequent carrier depletion. The effective carrier lifetime is the characteristic time of CDP. The intraband effects include spectral hole burning (SHB) and carrier heating (CH). These effects collectively contribute to FWM for signal-pump detunings below 4 THz,

For a pump wave at frequency ω_p and signal wave at frequency ω_s, the conjugate idler due to FWM is produced at $\omega_i = 2\omega_p - \omega_s$. This wave is not only at different frequency but is also the phase conjugated version of the signal wave. This is the FWM product that enables the use of nonlinear SOA for MSSI.

SOA as a nonlinear medium for optical signal processing offers several advantages over passive nonlinear devices like highly nonlinear fiber (HNLF). The conjugate product using FWM in SOA can be produced at low pump power levels and short interaction lengths. The gain medium of SOA enables high conversion efficiency, the ratio of the power of the generated conjugate idler to that of the input signal. However, due to the active nature of the device and strong nonlinear interactions, for MSSI application, amplified spontaneous emission noise (ASE) and nonlinear products within the signal band are points of concern, especially for CO-OFDM signals that are sensitive to nonlinearity. In this section, the performance of SOA for MSSI of OFDM signals is studied through simulations.

3.2.1 Simulation Model of SOA

Agrawal and Olsson (1989) give the mathematical model for SOA from fundamental carrier density rate equations. Under the assumptions that transverse carrier diffusion and group velocity dispersion are absent in the SOA, the medium can be described with the following set of equations,

$$\frac{\partial P}{\partial z} = (g - \alpha_{\text{int}})\, P \tag{3.3}$$

$$\frac{\partial \phi}{\partial z} = -\frac{1}{2}\alpha_{LW} g \tag{3.4}$$

$$\frac{\partial g}{\partial T} = \frac{g_0 - g}{\tau_c} - \frac{gP}{E_{\text{sat}}}. \tag{3.5}$$

where z, T are the space and time coordinates respectively (T is measured in a reference frame moving with the pulse), $A = \sqrt{P}\text{exp}(j\phi)$ is the envelope of the electric field,

$P = P(z,T)$ is the power, $\phi = \phi(z,T)$ is the phase, g is the saturated gain, α_{int} is the internal loss coefficient, g_0 is the small signal gain, α_{LW} is the linewidth expansion factor, τ_c is the spontaneous carrier lifetime and E_{sat} is the saturation energy of the amplifier.

The approximate solution to the above set of equations is,

$$P_{\text{out}}(T) = P_{\text{in}}(T)\text{exp}\left(h(T) - \alpha_{\text{int}}L\right) \tag{3.6}$$

$$\phi_{\text{out}}(T) = \phi_{\text{in}}(T) - \frac{1}{2}\alpha_{LW}h(T) \tag{3.7}$$

where the subscripts 'in' and 'out' refer to the value of the quantities at the input and output of the device, L is the length of the medium, $h(T)$ is the integrated gain over the length of the medium,

$$h(T) = \int_0^L g(z,T)dz \tag{3.8}$$

$$\frac{\partial h}{\partial T} = \frac{g_0 L - h}{\tau_c} - \frac{P_{\text{in}}(T)}{E_{\text{sat}}}\left(\exp(h) - 1\right). \tag{3.9}$$

Carrier heating and spectral hole burning $h(T)$ in the above analysis is the integrated gain assuming only carrier density pulsations. Carrier heating and spectral hole burning also affect the integrated gain. Under quasi-equilibrium conditions that the variations in $P(T)$ occur at time scales much larger than the characteristic time constants of carrier heating and spectral hole burning, Naimi *et al.* (2014) present the equations,

$$h_{ch}(T) = -\epsilon_{ch}\left[\exp(h(t)) - 1\right]P \tag{3.10}$$

$$h_{shb}(T) = -\epsilon_{shb}\left[\exp(h(t)) - 1\right]P \tag{3.11}$$

$$\begin{aligned} P_{\text{out}}(T) &= P_{\text{in}}(T)\text{exp}\left[h(T) + h_{ch}(T) + h_{shb}(T) - \alpha_{\text{int}}L\right] \\ \phi_{\text{out}}(T) &= \phi_{\text{in}}(T) - \frac{1}{2}\alpha_{LW}h(T) - \frac{1}{2}\alpha_{ch}h_{ch}(T). \end{aligned} \tag{3.12}$$

where ϵ_{ch} and ϵ_{shb} are the nonlinear gain suppression factors due to carrier heating and spectral hole burning respectively and α_{ch} is the carrier heating gain phase coupling factor. Equations (3.9 -3.12) are used to simulate signal propagation in SOA. The differential equation is solved numerically using the predictor-corrector method (Arfken and Weber (1999)).

3.2.2 Simulation of OPC for CO-OFDM in SOA

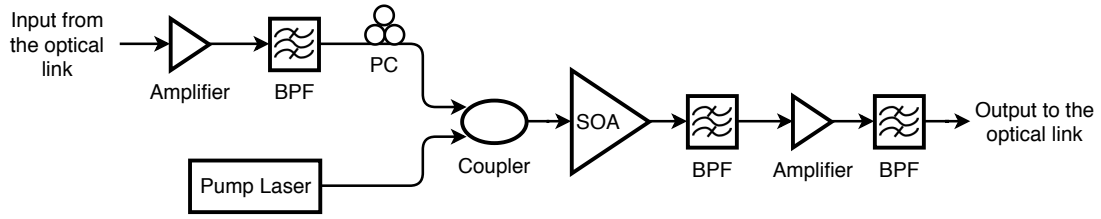

Figure 3.5: Schematic for OPC using SOA. BPF - Band-Pass Filter, PC - Polarization Controller.

The back-to-back performance of spectral inversion of CO-OFDM in SOA is studied through simulations. The parameters of the CO-OFDM signal are the same as given in table 3.1. The parameters of SOA are listed in table 3.2. The block diagram of the OPC module is shown in figure 3.5. The optical signal to be spectrally inverted is amplified to required power levels, filtered to remove out-of-band noise and combined with a co-polarized pump wave and launched into the input of the nonlinear SOA. The output of the SOA is filtered to obtain the conjugate idler, amplified and filtered to remove out-of-band noise.

Table 3.2: SOA parameters for simulation: MSSI using SOA

Parameter	Value
Unsaturated gain $g_0 L$	10
Internal loss $\alpha_{\text{int}} L$	4
Carrier lifetime τ_c	$25\,ps$
Saturation power $P_{\text{sat}} = E_{\text{sat}}/\tau_c$	$2\,mW$
Linewidth enhancement factor α_{LW}	4
Carrier heating nonlinear gain supression factor ϵ_{ch}	$0.5\,W^{-1}$
Spectral hole burning nonlinear gain supression factor ϵ_{shb}	$2\,W^{-1}$
Carrier heating gain phase coupling factor α_{ch}	0.5
Pump wave wavelength λ_p	$1550\,nm$
Pump signal detuning $\omega_p - \omega_s$	$-150\,GHz$
Pump laser linewidth $\Delta\nu_p$	$40\,kHz$
Signal laser linewidth $\Delta\nu_s$	$100\,kHz$

The OSNR of the generated optical OFDM signal is set at $26\,dB$, a typical OSNR value at the mid-span of the link. The pump and signal waves are coupled and launched into the SOA. The output is filtered to obtain the signal and the idler components. While idler is the product of interest, the signal is also processed to set a reference for performance comparison.

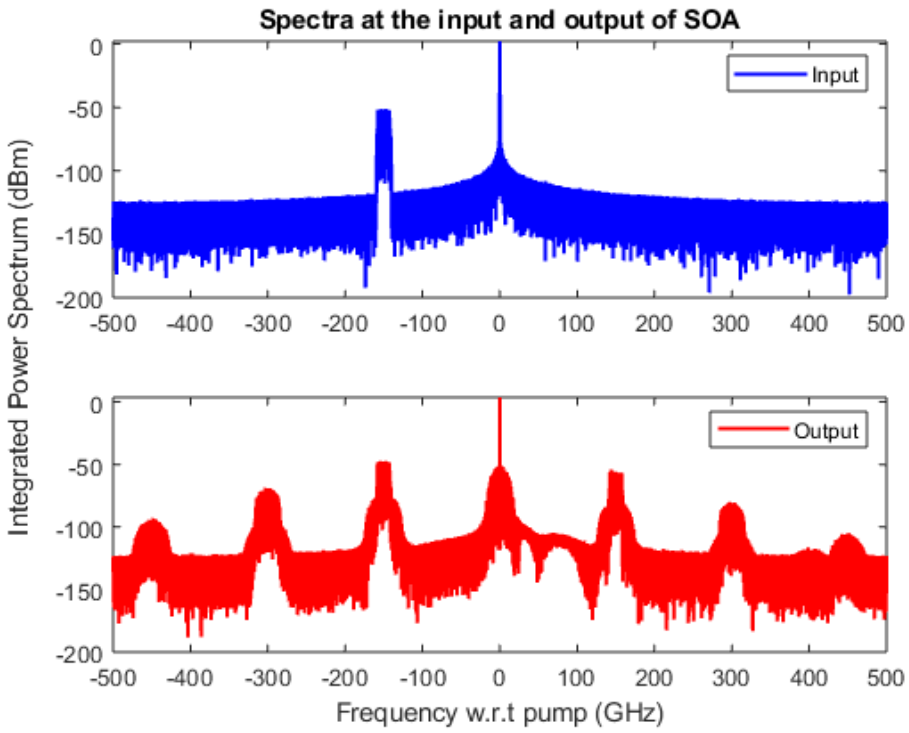

Figure 3.6: The input spectrum (top) shows the pump and signal at $-150\,GHz$ detuning. The output spectrum (bottom) has multiple idlers of which the conjugate idler at $150\,GHz$ detuning is used for MSSI.

Figure 3.6 shows the spectra at the input and the output of the SOA for $0\,dBm$ pump power and $-10\,dBm$ signal power. In the output spectra, the conjugate idler is obtained $150\,GHz$ away from the pump on the higher frequency side. This is the idler of interest, the other idlers generated in the medium are not conjugates of the signal. This idler is filtered, detected and processed at the receiver. At the receiver phase noise is mitigated using pilot aided CPE estimation technique.

Due to the FWM process, the phase of the idler is $\phi_i = 2\phi_p - \phi_s$ and the phase noise also follows the relation $\Delta\phi_i = 2\Delta\phi_p - \Delta\phi_s$. The linewidth (proportional to the variance of successive phase difference) follows the relation $\Delta\nu_i = 4\Delta\nu_p + \Delta\nu_s$. This is a major increase in the effective phase noise of the idler and causes a degradation in performance with respect to that of the signal.

To find a suitable operating point, the signal and the pump powers at the input of the SOA are varied and the performance studied. Figure 3.7 shows the EVM versus signal power curves for different pump powers. These curves are valid for any modulation format. The ideal EVM line for the input OSNR is marked for reference. The EVM curves for the signal component (at ω_s) fall slightly below their corresponding idler

(at ω_i) curves. This difference can be attributed to larger effective phase noise in the idler. For a given pump power, increasing the signal power results in higher EVM. For a given signal power, decreasing the pump power also results in higher EVM, This is due to pump induced SOA gain saturation. When the pump power is significantly higher than the signal power, the gain is predominantly controlled by the pump wave and this results in better EVM performance.

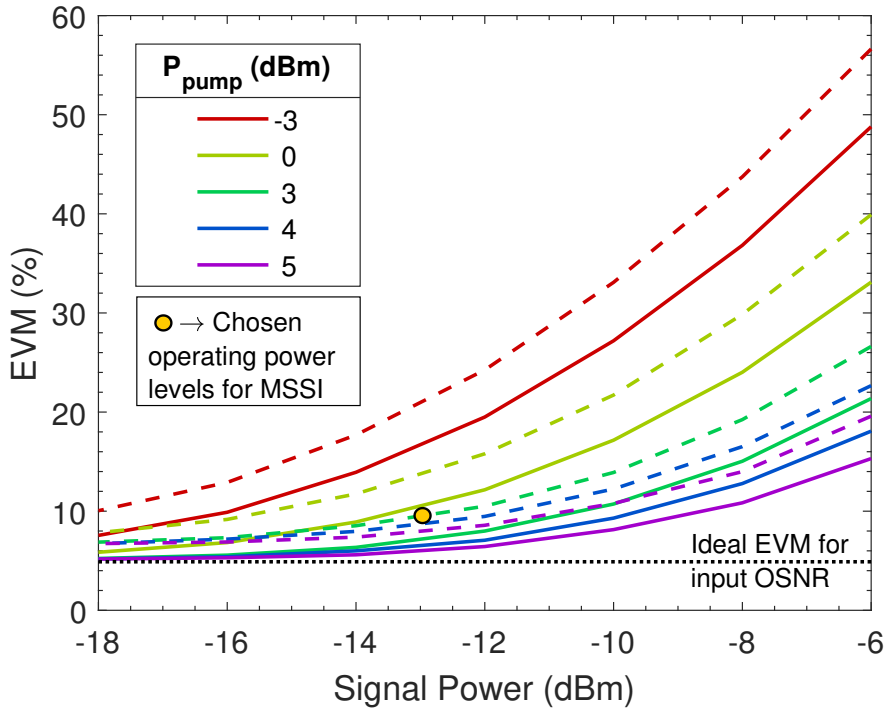

Figure 3.7: EVM performance of OPC of CO-OFDM signal in a back-to-back configuration for various signal and pump power levels. The solid curves correspond to the signal and the dashed curves correspond to the conjugate idler. The ideal EVM line for the input OSNR of $26\,dB$ is shown for reference.

If the input OSNR was lower than the chosen value, the reference line in figure 3.7 will move higher and all curves lying below this new reference will be pushed to the new reference line (performance is limited by noise at the input) but the curves lying above them will remain virtually undisturbed (performance is limited by the medium).

3.2.3 Simulation of MSSI of CO-OFDM system using SOA

A long haul CO-OFDM system with the parameters listed in table 3.1 is simulated with mid-span OPC using SOA with parameters listed in table 3.2. For the MSSI operation, the signal power at the input of the SOA is maintained at $-13\,dBm$ and pump power

at $3\,dBm$, this operating point is marked in the figure 3.7. The pump power can be increased but it is avoided because in a practical system there will be strict input power limitations. The OSNR at the transmitter is set at $30\,dB$.

The schematic of the system is similar to that of the ideal MSSI simulations (figure 3.1) but the ideal MSSI module is replaced by the OPC block using SOA (figure 3.5). The signal after traversing half the link is fed into the SOA-OPC module. The idler is filtered from the output of the SOA, suitably amplified and launched into the second half of the link. At the receiver there is no digital compensation for chromatic dispersion or nonlinearity. Timing and frequency synchronization is assumed to be perfect. The EVM performance is studied through these simulations. As a reference, the performance of CO-OFDM systems with Ideal MSSI (section 3.1) is used. To show the efficacy, the same link is simulated without MSSI and processed at the receiver with digital chromatic dispersion compensation using frequency domain equalizer.

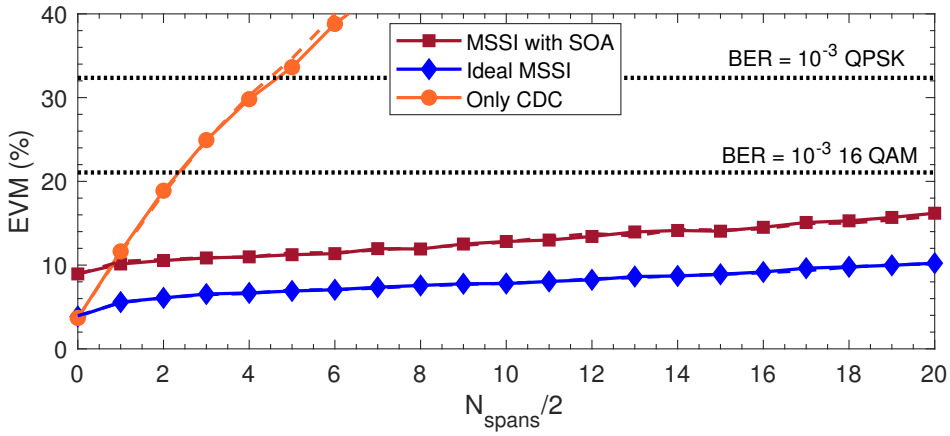

Figure 3.8: Effect of transmission distance on the EVM performance of MSSI using SOA; Signal launch power is $3\,dBm$; CDC - chromatic dispersion compensation. Solid lines correspond to QPSK and dashed lines correspond to 16 QAM

Figure 3.8 plots EVM as a function of the number of spans for a launch power of $3\,dBm$ for the schemes involving MSSI with SOA, with ideal MSSI and without MSSI (only CDC). We see that the EVM performance of SOA-MSSI has a penalty with respect to the ideal case due to spurious FWM components within the signal band. However, it performs very well in comparison to the non-MSSI case. For a BER of 10^{-3}, the EVM for QPSK is about 32% and for 16 QAM it is about 21%. If this BER is taken as the FEC limit, then without explicit nonlinearity compensation the reach is

limited to 10 spans for QPSK and 6 spans for 16 QAM for the given launch power level.

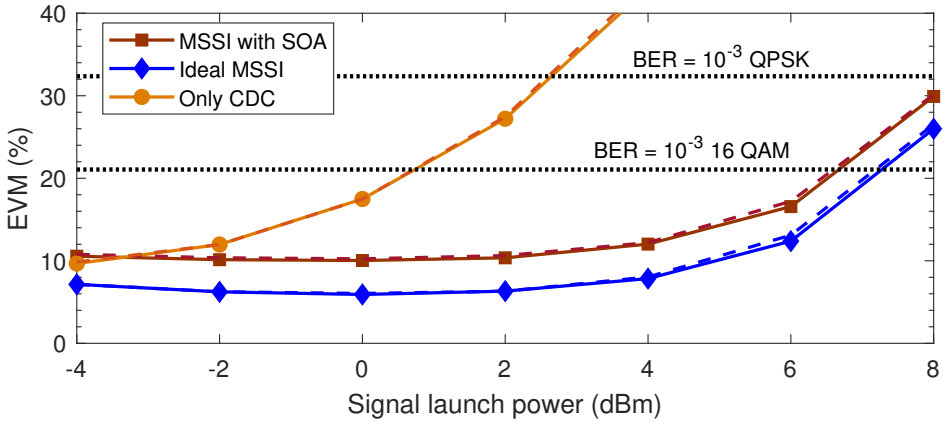

Figure 3.9: Effect of signal launch power on the EVM performance of MSSI using SOA; The transmission length is 800 km (10 spans) ; CDC - chromatic dispersion compensation.

The effect of launch power on the performance of the system is seen in figure 3.9. For the MSSI case, as the power increases, the EVM decreases and then increases: the EVM is almost constant for upto $4\,dBm$ launch power and then increases. This is the point where the residual nonlinear distortion starts to significantly affect the performance. For the non-MSSI case, the minima occurs outside the range of signal launch power considered. This illustrates the need for nonlinear mitigation - due to these power limitations, the throughput and reach of the link is limited. These simulations show the efficacy of MSSI as a nonlinear mitigation strategy and SOA as a suitable device for realizing it. This nonlinear mitigation would enable the transmission of more advanced modulation formats.

CHAPTER 4

CONCLUSION AND FUTURE WORK

In this report, the framework of coherent optical orthogonal frequency division multiplexing (CO-OFDM) was discussed. The elements of CO-OFDM - modulation and demodulation, coherent transmitter and receiver were explained in detail. The common impairments in a typical CO-OFDM system at the transmitter, receiver and channel level were examined and the ways to mitigate them were discussed. Through extensive simulations the working of the mitigation schemes were studied.

At the transmitter and receiver side, the impairments analysed in this report were carrier frequency offset and laser phase noise. For laser phase noise mitigation, CPE estimation using blind and pilot-aided techniques were studied. However in CO-OFDM systems, the effect of phase noise also manifests as ICI. As a future work, adaptive filters to mitigate ICI can be investigated. This will improve the performance beyond what is limited by the signal to interference and noise ratio (SINR). Furthermore, the hardware level impairments at the transmitter and receiver side were studied. These limit the achievable system performance and must be handled at the hardware level.

At the channel side, nonlinearity, chromatic dispersion and polarization dependent loss were the impairments considered. PDL compensation was achieved through the adaptation of space-time codes for PDM systems. While PDL can be reduced by careful design of individual inline polarization sensitive optical devices, these codes can be extended for MDM systems where fading is a more serious performance limiter. Nonlinearity and chromatic dispersion compensation using MSSI with SOA, an all-optical scheme, was discussed. The performance of single polarization CO-OFDM transmission was studied through simulations. This can be extended to polarization multiplexed, multichannel transmission with higher order modulation formats and more realistic factors like non-uniform fiber conditions and imperfections. Currently, researchers are trying to mitigate nonlinearity and dispersion using machine learning techniques (Zibar *et al.* (2016),Giacoumidis *et al.* (2017)). This can be used in conjugation with optical techniques like MSSI to handle residual distortions.

While this work has been completely simulation based, it provides insights into the working of a CO-OFDM system. The analysis would be complete when the impairment mitigation techniques are put to use in real systems. In practical systems, there are more challenges like timing synchronization, temporal variation of channel conditions and hardware limitations. Thus, extending the points of this study with experiments will be the next step. This will quantify the suitability of OFDM for optical communications.

APPENDIX A

Extension of space time codes for MDL mitigation

In chapter 2, the application of space time codes for PDL mitigation was discussed. A parallel was drawn from the MIMO model of a wireless fading channel and an optical fiber channel with PDL. Similarly, a parallel can be drawn to Mode Division Multiplexed (MDM) channels with Mode Dependent Loss (MDL). The MIMO model for each OFDM subcarrier equivalent to equation (2.21) for MDM systems for few mode fiber (FMF) with space time codes is (Awwad *et al.* (2015)),

$$\mathbf{Y}_{M\times T} = \mathbf{H}_{M\times M}\mathbf{X}_{M\times T} + \mathbf{N}_{M\times T} \tag{A.1}$$

where $\mathbf{X}_{M\times T}$ ($\mathbf{X}_{M\times T}$) is the transmitted (received) codeword for M spatial modes of fiber over T time slots, $\mathbf{H}_{M\times M}$ is the linear channel matrix, $\mathbf{N}_{M\times T}$ is the AWG noise matrix. The above equation omits laser phase noise and frequency offset effects and modal dispersion assuming a single wavelength narrow frequency flat channel. For L spans, the channel matrix can be written as,

$$\mathbf{H}_{M\times M} = \sqrt{\alpha}\prod_{l=1}^{L}(\mathbf{P}_l\mathbf{G}_l\mathbf{F}_l) \tag{A.2}$$

where $\mathbf{F}_l$ is the channel matrix considering the effect of the lth span, $\mathbf{G}_l$ is a diagonal matrix containing the gain coefficients of the Few Mode Amplifier (FMA) for the lth span, $\mathbf{P}_l$ is a random permutation matrix due to the scrambler and $\sqrt{\alpha}$ is the common normalization factor. Assuming that the fiber induced MDL is negligible (unitary mode coupling in the fiber) and that the MDL is induced due to inline components alone, each fiber span can be modeled as a series of K independent sections,

$$\mathbf{F}_{\text{span},M\times M} = \prod_{k=1}^{K}(\mathbf{T}_k\mathbf{R}_k) \tag{A.3}$$

where $\mathbf{T}_k$ is a diagonal matrix with random phase entries and $\mathbf{R}_k$ is a real orthogonal rotation matrix modeling the distributed modal crosstalk. The expression for $\mathbf{R}_k$ is

detailed in (Warm and Petermann (2013)) in terms of the misalignment σ of fiber core between the sections of the fiber.

Space time block codes (STBC) that has full rate should be used to benefit from multiplexing gain of MDM. One such family of codes is the linear threaded algebraic space time codes (TAST) (El Gamal and Damen (2003)). Square TAST codes can be used for a $M = T$ system. For a 3 spatial mode FMF ($LP_{01}, LP_{11a}, LP_{11b}$), we need a 6×6 TAST code. The codeword for a 6×6 TAST code is given as,

$$\mathbf{X}_{\mathscr{T},6\times 6} = \frac{1}{\sqrt{6}} \begin{bmatrix} f_1(\mathbf{s}_1) & \phi^{\frac{5}{6}} f_2(\mathbf{s}_6) & \phi^{\frac{4}{6}} f_3(\mathbf{s}_5) & \phi^{\frac{3}{6}} f_4(\mathbf{s}_4) & \phi^{\frac{2}{6}} f_5(\mathbf{s}_3) & \phi^{\frac{1}{6}} f_6(\mathbf{s}_2) \\ \phi^{\frac{1}{6}} f_1(\mathbf{s}_2) & f_2(\mathbf{s}_1) & \phi^{\frac{5}{6}} f_3(\mathbf{s}_6) & \phi^{\frac{4}{6}} f_4(\mathbf{s}_5) & \phi^{\frac{3}{6}} f_5(\mathbf{s}_4) & \phi^{\frac{2}{6}} f_6(\mathbf{s}_3) \\ \phi^{\frac{2}{6}} f_1(\mathbf{s}_3) & \phi^{\frac{1}{6}} f_2(\mathbf{s}_2) & f_3(\mathbf{s}_1) & \phi^{\frac{5}{6}} f_4(\mathbf{s}_6) & \phi^{\frac{4}{6}} f_5(\mathbf{s}_5) & \phi^{\frac{3}{6}} f_6(\mathbf{s}_4) \\ \phi^{\frac{3}{6}} f_1(\mathbf{s}_4) & \phi^{\frac{2}{6}} f_2(\mathbf{s}_3) & \phi^{\frac{1}{6}} f_3(\mathbf{s}_2) & f_4(\mathbf{s}_1) & \phi^{\frac{5}{6}} f_5(\mathbf{s}_6) & \phi^{\frac{4}{6}} f_6(\mathbf{s}_5) \\ \phi^{\frac{4}{6}} f_1(\mathbf{s}_5) & \phi^{\frac{3}{6}} f_2(\mathbf{s}_4) & \phi^{\frac{2}{6}} f_3(\mathbf{s}_3) & \phi^{\frac{1}{6}} f_4(\mathbf{s}_2) & f_5(\mathbf{s}_1) & \phi^{\frac{5}{6}} f_6(\mathbf{s}_6) \\ \phi^{\frac{5}{6}} f_1(\mathbf{s}_6) & \phi^{\frac{4}{6}} f_2(\mathbf{s}_5) & \phi^{\frac{3}{6}} f_3(\mathbf{s}_4) & \phi^{\frac{2}{6}} f_4(\mathbf{s}_3) & \phi^{\frac{1}{6}} f_5(\mathbf{s}_2) & f_6(\mathbf{s}_1) \end{bmatrix} \tag{A.4}$$

where $\mathbf{s}_k, k = 1, 2, \ldots, 6$ are vectors of 6 complex symbols each, $\phi = \exp(j\pi/12)$, $f_n(\mathbf{x}) = \sum_{k=1}^{6} x_k(\zeta^{n-1}\xi)^{k-1}$, $\zeta = \exp(j\pi/18)$, $\xi = \exp(j2\pi/6)$. 36 symbols map to a matrix codeword with 36 elements thus preserving the rate of coding.

The decoding is similar to that of polarization time codes. Maximum likelihood (ML) decoding rule is given as follows. The estimate $\hat{\mathbf{X}}_{ML}$ is given as,

$$\hat{\mathbf{X}}_{ML} = \underset{\mathbf{X}_{M\times T}\in\mathscr{C}}{\arg\min} ||\mathbf{Y} - \mathbf{H}\mathbf{X}||^2 \tag{A.5}$$

where $\mathscr{C}$ is the codeword space, a list of all possible transmitted codewords.

APPENDIX B

Blind phase noise mitigation: K4P

The algorithm for K4P, a blind phase noise mitigation technique for CO-OFDM systems is given in Algorithm 1. The measurement and process noise covariances Q and R are set according to the following relation.

Algorithm 1 K4P Algorithm

procedure F($\mathbf{S}$) ▷ Function to estimate CPE from $\mathbf{S}$ using fourth power technique
  $\theta_{\text{out}} \leftarrow \frac{1}{4}E\left\{\angle\left(\mathbf{S}^4\right) + \left(\angle\left(\mathbf{S}^4\right) \leq 0\right)\pi - \left(1 - \left(\angle\left(\mathbf{S}^4\right) \leq 0\right)\right)\pi\right\}$
  return θ_{out} ▷ The estimate is θ_{out}

procedure K4P($\mathbf{Y}_x, \mathbf{Y}_y, \theta_{x0}, \theta_{y0}, Q, R$) ▷ Received PDM signals after FFT $\mathbf{Y}_x, \mathbf{Y}_y$; first symbol CPE θ_{x0}, θ_{y0}; Kalman filter parameters Q, R
  $\hat{\theta}^x_{0|-1} \leftarrow \theta_{x0}$, $\hat{\theta}^y_{0|-1} \leftarrow \theta_{y0}$ ▷ Initialization of states
  $P^x_{0|-1} \leftarrow Q, P^y_{0|-1} \leftarrow Q$ ▷ Initialization of covariance
  for $k = 1, 2, \ldots, N_{\text{symb}}$ **do**
    $\mathbf{Z}_x \leftarrow \mathbf{Y}_x[k]\text{exp}\left(-j\hat{\theta}^x_{k|k-1}\right)$ ▷ Phase-slip prevention
    $\mathbf{Z}_y \leftarrow \mathbf{Y}_y[k]\text{exp}\left(-j\hat{\theta}^y_{k|k-1}\right)$ ▷ Phase-slip prevention
    $\mathbf{Y}_{\text{in}} \leftarrow \{u | u \in \mathbf{Z}_x \cup \mathbf{Z}_y, |u| \leq r^{\text{in}}_{th}\}$ ▷ Inner points, r^{in}_{th} is the threshold
    $\mathbf{Y}_{\text{out}} \leftarrow \{u | u \in \mathbf{Z}_x \cup \mathbf{Z}_y, |u| \geq r^{\text{out}}_{th}\}$ ▷ Outer points, r^{out}_{th} is the threshold
    $\hat{\theta}_{k,i} \leftarrow F(\mathbf{Y}_{\text{in}})$
    $\hat{\theta}_{k,o} \leftarrow F(\mathbf{Y}_{\text{out}})$
    $\hat{\theta}_{k,q} \leftarrow \gamma_w\hat{\theta}_{k,o} + (1 - \gamma_w)\hat{\theta}_{k,i}$ ▷ Multilevel QPSK partitioning
    for $p = x, y$ **do**
      $\hat{\theta}^p_{k,q} \leftarrow \hat{\theta}_{k,q} + \hat{\theta}^p_{k|k-1}$ ▷ Prediction Step
      $R^p_{E,k} \leftarrow P^p_{k|k-1} + R$
      $K^p_k \leftarrow P^p_{k|k-1}/R^p_{E,K}$
      $\hat{\theta}^p_{k+1|k} \leftarrow K^p_k\left(\hat{\theta}^p_{k,q} - \hat{\theta}^p_{k|k-1}\right)$
      $\mathbf{Y}_p[k] \leftarrow \mathbf{Y}_p[k]\text{exp}\left(-j\hat{\theta}^x_{k+1|k}\right)$
      $P^p_{k+1|k} \leftarrow P^p_{k|k-1}\left(1 - K^p_k\right) + Q$
  return $\mathbf{Y}_x, \mathbf{Y}_y$ ▷ The CPE compensated signals

$$\begin{aligned} Q &= 2\pi\Delta\nu T_s \\ R &= \frac{\eta}{\text{OSNR}} \end{aligned} \tag{B.1}$$

where η is the reciprocal of the average number of points to average. The covariances are only ball-park estimates. As Kalman filter is adaptive in nature, this should suffice.

APPENDIX C

MATLAB codes for the simulation

C.1 OFDM data generation and demodulation

```
% Author     : Lakshmi Narayanan V, Anirudh Vijay
% Institute : Indian institute of technology Madras, Chennai
% Function to generate OFDM signal
% Sample OFDM_param:
%%%%%%%%%%%%%%%%%%%%% OFDM Parameters %%%%%%%%%%%%%%%%%%%%%
% OFDM_param.Nfft           = 64;           % Total # of subcarriers
% OFDM_param.Nsymb          = 2^11;         % Total # Symbols in one frame
% OFDM_param.ModOrder       = 2;            % 4 for 16-QAM, 2 for QPSK
% OFDM_param.RSamp          = 20;           % OFDM System Frequency in GS/s
% OFDM_param.DACSamp        = 60;           % OFDM DAC Sampling Rate in GS/s
% OFDM_param.Nt             = OFDM_param.DACSamp/...
%                               OFDM_param.RSamp;% Over Sampling Ratio
% OFDM_param.BandWidth      = 16;       % Required transmission BW in GHz
% OFDM_param.NPilots        = 8; % Total # Pilots
% OFDM_param.DataSubCr      = ceil((OFDM_param.BandWidth * OFDM_param.Nfft)...
%     /OFDM_param.RSamp) - OFDM_param.NPilots; % Total # of data subcarriers
% OFDM_param.PRBSOrder      = 11;       % PRBS order
% OFDM_param.Ncp            = 8; % Total # Subcarrier in Cyclic Prefix
% OFDM_param.ClipRatio      = 4; % Total # Subcarrier in Cyclic Prefix
%
% OFDM_param.PilotsPeriod   = ceil(OFDM_param.DataSubCr/OFDM_param.NPilots);
% OFDM_param.DC             = 1; % DC Component
% OFDM_param.DC_NullBand    = 0; % Total # of zero subcarriers near DC
%% Total # of data subcarriers, Left to DC
% OFDM_param.DataSubCr_L    = ceil(OFDM_param.DataSubCr/2);
%% Total # of data subcarriers, Right to DC
% OFDM_param.DataSubCr_R    = OFDM_param.DataSubCr - OFDM_param.DataSubCr_L;
%% Total # of Guard Band  subcarriers, Left to DC
% OFDM_param.GuardBand_L    = ceil(OFDM_param.Nfft/2) - ...
%     OFDM_param.DataSubCr_L - (OFDM_param.DC_NullBand/2) - ...
%     (OFDM_param.NPilots/2);
```

```
%% Total # of Guard Band  subcarriers, Right to DC
% OFDM_param.GuardBand_R    = ceil(OFDM_param.Nfft/2) - ...
%       OFDM_param.DataSubCr_R - (OFDM_param.DC_NullBand/2) - ...
%       (OFDM_param.NPilots/2) -1;

function [OFDM_MOD_DATA, Ordered_Bit_INPUT,...
    QAMMOD_DATA_SYMB,QAMMOD_PILOT_SYMB] = OFDM_Data_Generation(OFDM_param)
% global OFDM_param
bit_length          = OFDM_param.ModOrder * OFDM_param.Nsymb * ...
    OFDM_param.DataSubCr;
PRBS_set            = idinput((2^OFDM_param.PRBSOrder-1),'prbs',[0 1],[0 1]);
Rep_Factor          = ceil(bit_length/(2^OFDM_param.PRBSOrder-1));
PRBS_bit_sequence = repmat(PRBS_set,Rep_Factor,1);
PRBS_bit_sequence = PRBS_bit_sequence(1:bit_length);
Ordered_Bit_INPUT = reshape(PRBS_bit_sequence,[(OFDM_param.DataSubCr ...
    * OFDM_param.ModOrder) (OFDM_param.Nsymb)]);
QAMMOD_DATA_SYMB  = qammod(Ordered_Bit_INPUT,2^(OFDM_param.ModOrder),...
    'UnitAveragePower',true,'InputType','bit');
QAMMOD_DATA_DEC   = qamdemod(QAMMOD_DATA_SYMB,2^(OFDM_param.ModOrder),...
    'UnitAveragePower',true);

if OFDM_param.NPilots~=0
    QAMMOD_PILOT_SYMB = qammod(randi([0,3],OFDM_param.NPilots,...
        OFDM_param.Nsymb),4,'UnitAveragePower',true);
else
    QAMMOD_PILOT_SYMB = [];
end
%%
OFDM_param.SymbolLocData = ...
    [zeros(OFDM_param.GuardBand_L,OFDM_param.Nsymb);...
    QAMMOD_DATA_SYMB(1:OFDM_param.DataSubCr_L  ,:);...
    zeros((OFDM_param.DC_NullBand/2),OFDM_param.Nsymb);...
    zeros(OFDM_param.DC  ,OFDM_param.Nsymb);...
    zeros((OFDM_param.DC_NullBand/2),OFDM_param.Nsymb);...
    QAMMOD_DATA_SYMB(OFDM_param.DataSubCr_L+1:end  ,:);...
    zeros(OFDM_param.GuardBand_R,OFDM_param.Nsymb)];


%% Inserting the Pilot Subcarriers
Nfft_Subcarriers = 1:OFDM_param.Nfft;
```

```
OFDM_param.Pilot_rows = ceil(OFDM_param.Nfft/2) - ...
    [OFDM_param.PilotsPeriod*(1:OFDM_param.NPilots/2)+1 ...
    OFDM_param.PilotsPeriod*(-OFDM_param.NPilots/2:-1)];
OFDM_param.Data_OFDM = zeros(OFDM_param.Nfft,OFDM_param.Nsymb);

OFDM_param.Data_OFDM(OFDM_param.Pilot_rows,:) = QAMMOD_PILOT_SYMB;

Data_OFDM = OFDM_param.Data_OFDM;
Data_OFDM(setdiff(Nfft_Subcarriers,OFDM_param.Pilot_rows),:) ...
    = OFDM_param.SymbolLocData;
%% OFDM Modulation
OFDM_MOD_DATA = ifft(ifftshift(Data_OFDM,1))*sqrt(OFDM_param.Nfft);

%% Adding cyclic prefix
if OFDM_param.Ncp~=0
    OFDM_MOD_DATA = reshape([OFDM_MOD_DATA(end-OFDM_param.Ncp+1:end,:);...
        OFDM_MOD_DATA],[],1);
end
OFDM_MOD_DATA = reshape(OFDM_MOD_DATA./...
    sqrt(mean(mean(abs(OFDM_MOD_DATA).^2))),[],1);
end
% ------------------------------------------------------------------------
% Author    : Anirudh Vijay, Lakshmi Narayanan V
% Institute : Indian institute of technology Madras, Chennai
% Function to demodulate OFDM signal
function [Ordered_Bit_OUTPUT,RX_QAMMOD_DATA_SYMB,Channel_Estimate] = ...
    OFDM_Data_Demodulation_EQ_v2_pilots(RxData_OFDM,QAMMOD_PILOT_SYMB,...
    OFDM_param,Data_OFDM,QAMMOD_DATA_SYMB)

RxData_OFDM             = reshape(RxData_OFDM,(OFDM_param.Nfft + ...
    OFDM_param.Ncp),[]);
RxData_OFDM             = RxData_OFDM(OFDM_param.Ncp + 1:end,:);
%%
L_dataSC_start_index  = OFDM_param.GuardBand_L +1;
L_dataSC_end_index    = OFDM_param.GuardBand_L + OFDM_param.DataSubCr_L;
R_dataSC_start_index  = L_dataSC_end_index + OFDM_param.DC + ...
    OFDM_param.DC_NullBand+1;
R_dataSC_end_index    = R_dataSC_start_index + OFDM_param.DataSubCr_R -1;
Nfft_Subcarriers      = 1:OFDM_param.Nfft;
OFDM_param.Pilot_rows = ceil(OFDM_param.Nfft/2) - ...
```

```
    [OFDM_param.PilotsPeriod*(1:OFDM_param.NPilots/2)+1  ...
    OFDM_param.PilotsPeriod*(-OFDM_param.NPilots/2:-1)];
data_GB_rows            = (setdiff(Nfft_Subcarriers,OFDM_param.Pilot_rows));
data_rows               = data_GB_rows([L_dataSC_start_index:...
    L_dataSC_end_index  R_dataSC_start_index:R_dataSC_end_index]);
%% Channel Estimation
Data_Pilot_DEMOD_OFDM = fftshift(fft(RxData_OFDM),1);
RX_Data_OFDM_Check    = Data_Pilot_DEMOD_OFDM./rms(Data_Pilot_DEMOD_OFDM);
Channel_Estimate      = ones(OFDM_param.Nfft,1);
Channel_Estimate(data_rows) = mean(RX_Data_OFDM_Check(data_rows,1:10)./...
    QAMMOD_DATA_SYMB(:,1:10),2);
Channel_Estimate(OFDM_param.Pilot_rows) = ...
    mean(RX_Data_OFDM_Check(OFDM_param.Pilot_rows,1:10)./...
    QAMMOD_PILOT_SYMB(:,1:10),2);
Data_Pilot_DEMOD_OFDM = Data_Pilot_DEMOD_OFDM./Channel_Estimate;
figure()
stem(abs(Channel_Estimate(data_rows)),'r')
%% Extracting the Pilot information
Rx_PILOT_SYMB           = Data_Pilot_DEMOD_OFDM(OFDM_param.Pilot_rows,:);
%% Extracting the Data subcarriers from the received OFDM symbol
Data_DEMOD_OFDM         = Data_Pilot_DEMOD_OFDM(setdiff(...
    Nfft_Subcarriers,OFDM_param.Pilot_rows),:);
RX_QAMMOD_DATA_SYMB     = Data_DEMOD_OFDM(...
    [L_dataSC_start_index:L_dataSC_end_index   ...
    R_dataSC_start_index:R_dataSC_end_index],:);
RX_QAMMOD_DATA_SYMB1    = RX_QAMMOD_DATA_SYMB./...
    sqrt(mean(mean(abs(RX_QAMMOD_DATA_SYMB).^2)));

if OFDM_param.NPilots~=0
    complex_rotation_est = ...
        exp(1j*angle(mean(Rx_PILOT_SYMB./QAMMOD_PILOT_SYMB)));
else
    complex_rotation_est = 1;
end
RX_QAMMOD_DATA_SYMB_PNcorr = RX_QAMMOD_DATA_SYMB1./complex_rotation_est;
%%
Ordered_Bit_OUTPUT = qamdemod(RX_QAMMOD_DATA_SYMB_PNcorr,...
    2^(OFDM_param.ModOrder),'UnitAveragePower',true,'OutputType','bit');
RX_QAMMOD_DATA_SYMB = RX_QAMMOD_DATA_SYMB_PNcorr;
figure()
```

```
delx = RX_QAMMOD_DATA_SYMB - QAMMOD_DATA_SYMB;
 evm_sc = rms(delx,2)*100;
stem(evm_sc,'b')
end
```

C.2 Chromatic dispersion compensation

```
% Author     : Lakshmi Narayanan V
% Institute : Indian institute of technology Madras, Chennai
% Function to compensate for CD given the dispersion parameter (disp) and
% length of transmission (len). omega = 2*pi*f, f in GHz
function [RX_sig] = cd_compensation(RX_sig,lambda,disp,len,omega,CLIGHT)
beta2 = lambda^2/2/pi/CLIGHT*disp*1e-6;
betat = 0.5*omega.^2*beta2;
combeta=betat*len;   %% total dispersion
Hx=fastexp(combeta);
ux = fft(RX_sig);
ux1 = Hx.*ux;
RX_sig = ifft(ux1);
end
```

C.3 Frequency offset compensation

```
% Author     : Lakshmi Narayanan V
% Institute : Indian institute of technology Madras, Chennai
function [RX_sig_compensated,freq_error_Hz] = ...
    FO_compensation(RX_OFDM_sig,symbrate,Nt)
Fs            = symbrate*Nt*1e9;
[mm,loc]      = max(fftshift(abs(fft(RX_OFDM_sig.^4-mean(RX_OFDM_sig.^4)))));
df = Fs/length(RX_OFDM_sig);
f_axis = (-Fs/2):df:(Fs/2-df);

freq_error     = (1/4)*(loc-1-length(RX_OFDM_sig)/2)/length(RX_OFDM_sig);
freq_error_Hz = (freq_error)*Fs; % freq_error unit [Hz/sample]
RX_sig_compensated = RX_OFDM_sig.*exp(-1i*2*pi*freq_error_Hz*...
    (0:(length(RX_OFDM_sig)-1))'/Fs);
end
```

C.4 Polarization time codes

```
% Function to map symbols to Silver Code
function x_out = silver(x_in)
z = [1+1j -1+2j; 1+2j 1-1j]*x_in(3:4,:)/sqrt(7);

x_out = [(x_in(1,:) + z(1,:));
         -conj(x_in(2,:)+z(2,:));
          (x_in(2,:)-z(2,:));
          conj(x_in(1,:) - z(1,:))]/sqrt(2);
end
% ------------------------------------------------------------------------
% Function to decode the received symbols given the channel matrix (H)
function [X_hat,bits_hat] = silver_demod_set(Y_rx,H)
[S,s_in] = silver_space();
Y_all = [H(1,1)*S(1:2,:) + H(1,2)*S(3:4,:);
         H(2,1)*S(1:2,:) + H(2,2)*S(3:4,:)];

X_hat = zeros(size(Y_rx));
for ii = 1:size(Y_rx,2)
    delY = Y_rx(:,ii) - Y_all;
    dists = sum(abs(delY).^2);
    [~,ind] = min(dists);
    X_hat(:,ii) = s_in(:,ind);
end

bits_hat = qamdemod(X_hat,4,'UnitAveragePower',...
    true,'OutputType','bit');
end
% ------------------------------------------------------------------------
% Function to simulate PT-codes in an OFDM system as parallel channels for
% a given SNR set (snr_dB) and channel matrix (H.
function [ber_unc,ber_silver,ber_ideal]=simulate_txrx_pdl(H,num,snr_db)
% Generating the QPSK symbols
ints = randi([0,3],4,num);
x = qammod(ints,4)/sqrt(2);
e = sqrt(eig(H*H'));
% Effect of Channel
x_ps = e.*[reshape(x(1:2,:),1,[]);reshape(x(3:4,:),1,[])];
x_ps = reshape(x_ps,1,[]);
```

```
bits = qamdemod(x,4,'UnitAveragePower',true,'OutputType','bit');

% Mapping to silver code
X = silver(x);

% Effect of Channel
X_ps = e.*[reshape(X(1:2,:),1,[]);reshape(X(3:4,:),1,[])];
H = diag(e);
ber_unc = zeros(size(snr_db));
ber_silver = ber_unc;

for ii = 1:length(snr_db)
    % Noise addition according to SNR
    y = awgn(x_ps,snr_db(ii));
    y_sp = [y(1:4:end);y(3:4:end);y(2:4:end);y(4:4:end)];
    Y = awgn(X_ps,snr_db(ii));

    Y_sp = [reshape(Y(1,:),2,[]);reshape(Y(2,:),2,[])];

    % Demodulation
    bits_unc_hat = qamdemod(y_sp,4,'UnitAveragePower',...
        true,'OutputType','bit');
    [~,bits_silver_hat] = silver_demod_set(Y_sp,H);

    ber_unc(ii) = sum(sum(bits~=bits_unc_hat))/numel(bits);
    ber_silver(ii) = sum(sum(bits~=bits_silver_hat))/numel(bits);
end

ebn0 = db2pow(snr_db)/2;
ber_ideal = 0.5*erfc(sqrt(ebn0));
end
```

C.5 Laser phase noise mitigation

```
% Authors: Anirudh Vijay, Lakshmi Narayanan V
% Institute: Indian institute of technology Madras, Chennai
% Function to implement K4P CPE correction
function [Rx_OFDM_freq_x,Rx_OFDM_freq_y,kal_ph] = ...
    PN_compensation_OFDM_PM(Rx_OFDM_freq_x,Rx_OFDM_freq_y,...
    OFDM_param,init_theta_x,init_theta_y,params)
```

```
A = 1;
Q = params(1);
R = params(2);
K = 1;
P = 1;
H = 1;
Rx_OFDM_freq_x = Rx_OFDM_freq_x./rms(Rx_OFDM_freq_x);
Rx_OFDM_freq_y = Rx_OFDM_freq_y./rms(Rx_OFDM_freq_y);

kal_ph = zeros(1,OFDM_param.Nsymb);
phi_apriori = 0;
if OFDM_param.ModOrder == 4
    ratio = 0.75;
elseif OFDM_param.ModOrder == 6
    ratio = 7/8;
else
    ratio = 1;
end



Rx_OFDM_freq_x(:,1) = Rx_OFDM_freq_x(:,1)*...
    exp(-1j*(phi_apriori+init_theta_x));
Rx_OFDM_freq_y(:,1) = Rx_OFDM_freq_y(:,1)*...
    exp(-1j*(phi_apriori+init_theta_y));
kal_ph(1) = phi_apriori;
for ii = 2:OFDM_param.Nsymb
    % Phase slip prevention
    y_x = Rx_OFDM_freq_x(:,ii)*exp(-1j*(phi_apriori+init_theta_x));
    y_y = Rx_OFDM_freq_y(:,ii)*exp(-1j*(phi_apriori+init_theta_y));
    k = ceil(4/2^OFDM_param.ModOrder*0.9*OFDM_param.DataSubCr);
    y = [y_x;y_y];

    % QPSK partitioning
    [~,ind1] = maxk(abs(y),k);
    [~,ind2] = mink(abs(y),k);
    outer_pts = y(ind1);
    inner_pts = y(ind2);
    angle_y4_outer = angle(outer_pts.^4);
    angle_y4_inner = angle(inner_pts.^4);
    theta_est_outer = mean(angle_y4_outer +  ...
```

```
        (angle_y4_outer<=0)*pi - (1-(angle_y4_outer<=0))*pi)/4;
    theta_est_inner = mean(angle_y4_inner + ...
        (angle_y4_inner<=0)*pi - (1-(angle_y4_inner<=0))*pi)/4;
    theta_est_0 = theta_est_inner*(1-ratio) + theta_est_outer*ratio;

    % Kalman filter
    apriori_ErrorCovariance = A*P*A' + Q;
    K = apriori_ErrorCovariance*H'/(H*apriori_ErrorCovariance*H' + R);

    phi_apriori = phi_apriori + K*theta_est_0;
    kal_ph(ii)=(phi_apriori);

    Rx_OFDM_freq_x(:,ii) = Rx_OFDM_freq_x(:,ii)*...
        exp(-1j*(phi_apriori+init_theta_x));
    Rx_OFDM_freq_y(:,ii) = Rx_OFDM_freq_y(:,ii)*...
        exp(-1j*(phi_apriori+init_theta_y));
    P = apriori_ErrorCovariance - K*H*apriori_ErrorCovariance;

end
end
%-------------------------------------------------------------------------
% Function to demodulate received PDM OFDM sigal with phase
% noise mitigation
function [Ordered_Bit_OUTPUT_x,Ordered_Bit_OUTPUT_y,...
    RX_QAMMOD_DATA_SYMB_x,RX_QAMMOD_DATA_SYMB_y,ph_err] = ...
    OFDM_Data_Demodulation_EQ_PN_PM(RxData_OFDM_x,RxData_OFDM_y,...
    QAMMOD_PILOT_SYMB_x,QAMMOD_PILOT_SYMB_y, OFDM_param,...
    Data_OFDM_x,Data_OFDM_y,first_data_x,first_data_y,...
    data_symb_x,data_symb_y,kal_params)
%% Serial to Parallel
RxData_OFDM_x   = reshape(RxData_OFDM_x,...
    (OFDM_param.Nfft + OFDM_param.Ncp),[]);
RxData_OFDM_x   = RxData_OFDM_x(OFDM_param.Ncp + 1:end,:);

RxData_OFDM_y   = reshape(RxData_OFDM_y,...
    (OFDM_param.Nfft + OFDM_param.Ncp),[]);
RxData_OFDM_y   = RxData_OFDM_y(OFDM_param.Ncp + 1:end,:);

L_dataSC_start_index  = OFDM_param.GuardBand_L +1;
L_dataSC_end_index    = OFDM_param.GuardBand_L + OFDM_param.DataSubCr_L;
```

```
R_dataSC_start_index  = L_dataSC_end_index + OFDM_param.DC + ...
    OFDM_param.DC_NullBand+1;
R_dataSC_end_index    = R_dataSC_start_index + OFDM_param.DataSubCr_R -1;
Nfft_Subcarriers      = 1:OFDM_param.Nfft;
OFDM_param.Pilot_rows = ceil(OFDM_param.Nfft/2) - ...
    [OFDM_param.PilotsPeriod*(1:OFDM_param.NPilots/2)+1 ...
    OFDM_param.PilotsPeriod*(-OFDM_param.NPilots/2:-1)];
data_GB_rows          = (setdiff(Nfft_Subcarriers,OFDM_param.Pilot_rows));
data_rows             = data_GB_rows([L_dataSC_start_index:...
    L_dataSC_end_index  R_dataSC_start_index:R_dataSC_end_index]);
%% FFT
Data_Pilot_DEMOD_OFDM_x = fftshift(fft(RxData_OFDM_x),1);
Data_Pilot_DEMOD_OFDM_y = fftshift(fft(RxData_OFDM_y),1);

%% Extracting the Pilot information
Rx_PILOT_SYMB_x         = Data_Pilot_DEMOD_OFDM_x(OFDM_param.Pilot_rows,:);
Rx_PILOT_SYMB_y         = Data_Pilot_DEMOD_OFDM_y(OFDM_param.Pilot_rows,:);
%% Extracting the Data subcarriers from the received OFDM symbol
Data_DEMOD_OFDM_x       = Data_Pilot_DEMOD_OFDM_x(setdiff(...
    Nfft_Subcarriers,OFDM_param.Pilot_rows),:);
RX_QAMMOD_DATA_SYMB_x   = Data_DEMOD_OFDM_x([L_dataSC_start_index:...
    L_dataSC_end_index  R_dataSC_start_index:R_dataSC_end_index],:);
RX_QAMMOD_DATA_SYMB_x1  = RX_QAMMOD_DATA_SYMB_x./...
    sqrt(mean(mean(abs(RX_QAMMOD_DATA_SYMB_x).^2)));

Data_DEMOD_OFDM_y       = Data_Pilot_DEMOD_OFDM_y(setdiff(...
    Nfft_Subcarriers,OFDM_param.Pilot_rows),:);
RX_QAMMOD_DATA_SYMB_y   = Data_DEMOD_OFDM_y([L_dataSC_start_index:...
    L_dataSC_end_index  R_dataSC_start_index:R_dataSC_end_index],:);
RX_QAMMOD_DATA_SYMB_y1  = RX_QAMMOD_DATA_SYMB_y./...
    sqrt(mean(mean(abs(RX_QAMMOD_DATA_SYMB_y).^2)));

% Pilot aided technique
if OFDM_param.NPilots~=0
    complex_rotation_est_x = exp(1j*angle(mean(Rx_PILOT_SYMB_x./...
        QAMMOD_PILOT_SYMB_x)));
    complex_rotation_est_y = exp(1j*angle(mean(Rx_PILOT_SYMB_y./...
        QAMMOD_PILOT_SYMB_y)));
else
    complex_rotation_est_x = 0;
```

```
    complex_rotation_est_y = 0;
end
first_symb_complx_rotation_x = angle(mean(RX_QAMMOD_DATA_SYMB_x1(:,1)./...
    first_data_x));
first_symb_complx_rotation_y = angle(mean(RX_QAMMOD_DATA_SYMB_y1(:,1)./...
    first_data_y));
% Blind K4P algorithm
[Rx_OFDM_freq_x,Rx_OFDM_freq_y,kal_ph] = ...
    PN_compensation_OFDM_PM(RX_QAMMOD_DATA_SYMB_x1,RX_QAMMOD_DATA_SYMB_y1,...
    OFDM_param,first_symb_complx_rotation_x,...
    first_symb_complx_rotation_y,kal_params);
ph_err = kal_ph;
RX_QAMMOD_DATA_SYMB_PNcorr_x = Rx_OFDM_freq_x;
RX_QAMMOD_DATA_SYMB_PNcorr_y = Rx_OFDM_freq_y;
%% Demodulation
Ordered_Bit_OUTPUT_x = qamdemod(RX_QAMMOD_DATA_SYMB_PNcorr_x,...
    2^(OFDM_param.ModOrder),'UnitAveragePower',true,'OutputType','bit');
RX_QAMMOD_DATA_SYMB_x = RX_QAMMOD_DATA_SYMB_PNcorr_x;

Ordered_Bit_OUTPUT_y = qamdemod(RX_QAMMOD_DATA_SYMB_PNcorr_y,...
    2^(OFDM_param.ModOrder),'UnitAveragePower',true,'OutputType','bit');
RX_QAMMOD_DATA_SYMB_y = RX_QAMMOD_DATA_SYMB_PNcorr_y;
end
```

C.6 SOA model

```
%Author Sean O Duill
function [ hdot ] = dhdt( soa, p_in, h_in )
% calculates the SOA rate equation for the time
% derivative for the SOA gain coefficient

hdot = (soa.h0 - h_in)/soa.tau_s - (h_in/(h_in-soa.loss))*...
    p_in*(exp(h_in-soa.loss)-1)/(soa.p_sat*soa.tau_s);
end
% ------------------------------------------------------------------------
%Author Sean O Duill
function [ h_new ] = solve_h( soa, timestep, p_in, h_in)
%Predictor-Corrector method to solve for h
%   calculate one euler step, use this value to perform another euler step.
%   then the updated value for h depends on the average of these two values
```

```
dh1 = dhdt(soa, p_in, h_in);
h_dash = dh1*timestep + h_in;
dh2 = dhdt(soa, p_in, h_dash);
h_new = 0.5*(dh1+dh2)*timestep + h_in;
end
% ------------------------------------------------------------------------
function [ soa_out_field] = soa_block( soa,timestep, e_in )
% This function reads in a electric field signal and calculates the
% output electric field signal at the output of an SOA. input electric
% field assumed to be complex in nature due to advanced md. formats.
% timestep = 1e-12; % determines the signal sampling rate and the timestep
% to solve SOA rate equation
% soa = soa_spec ;%soa = struct( 'loss', 2, 'h0', 8, 'alpha', 4, ...
% 'tau_s', 'p_sat', 0.01); % soa paramters loss, unsaturated gain coeff,
% alpha factor, , carrier lifetime, and saturation power

N = length(e_in);
p_in = abs(e_in).^2;% calculate the power (intensity) of the incoming wave;
h_t = zeros(1,N); %create array for h(t)
h_in = soa.h0; % Initialise h to be the unsaturated gain coefficient

for a = 1:N %calculates the SOA gain as a function of time
    h_t(a) = solve_h(soa, timestep, p_in(a), h_in);
    h_in = h_t(a); % updates h
end

del_h_ch =-1*h_t./(h_t-soa.loss).*(exp(h_t-soa.loss)-1).*p_in*soa.eps_ch;
del_h_shb =-1*h_t./(h_t-soa.loss).*(exp(h_t-soa.loss)-1).*p_in*soa.eps_shb;

% multiply the input field by the complex valued SOA gain
% (including alpha) to get the output field
soa_out_field = e_in.*exp(0.5*(-1*soa.loss + h_t.*(1-1i*soa.alpha)+...
    del_h_ch.*(1-1i*soa.alpha_ch)+del_h_shb.*soa.eps_shb));

end
```

REFERENCES

1. **Agrawal, G. P.** (1988). Population pulsations and nondegenerate four-wave mixing in semiconductor lasers and amplifiers. *JOSA B*, **5**(1), 147–159.

2. **Agrawal, G. P.**, *Fiber-optic communication systems*, volume 222. John Wiley & Sons, 2012.

3. **Agrawal, G. P.** and **N. A. Olsson** (1989). Self-phase modulation and spectral broadening of optical pulses in semiconductor laser amplifiers. *IEEE Journal of Quantum Electronics*, **25**(11), 2297–2306.

4. **Arfken, G. B.** and **H. J. Weber** (1999). Mathematical methods for physicists.

5. **Armstrong, J.** (2009). Ofdm for optical communications. *Journal of lightwave technology*, **27**(3), 189–204.

6. **Awwad, E.**, **Y. Jaouën**, and **G. R.-B. Othman** (2013). Polarization-time coding for pdl mitigation in long-haul polmux ofdm systems. *Opt. Express*, **21**(19), 22773–22790. URL `http://www.opticsexpress.org/abstract.cfm?URI=oe-21-19-22773`.

7. **Awwad, E.**, **G. R.-B. Othman**, and **Y. Jaouën** (2015). Space-time coding schemes for mdl-impaired mode-multiplexed fiber transmission systems. *Journal of Lightwave Technology*, **33**(24), 5084–5094.

8. **Bosco, G.**, **A. Carena**, **V. Curri**, **P. Poggiolini**, and **F. Forghieri** (2010). Performance limits of nyquist-wdm and co-ofdm in high-speed pm-qpsk systems. *IEEE Photonics Technology Letters*, **22**(15), 1129–1131.

9. **Cisco** (2019). Cisco Visual Networking Index: Forecast and Trends, 2017-2022 White Paper. Technical report. URL `https://www.cisco.com/c/en/us/solutions/collateral/service-provider/visual-networking-index-vni/white-paper-c11-741490.pdf`.

10. **Damen, O.**, **A. Chkeif**, and **J. . Belfiore**, Sphere decoding of space-time codes. *In 2000 IEEE International Symposium on Information Theory (Cat. No.00CH37060)*. 2000.

11. **Desbruslais, S. R.** and **P. R. Morkel**, Simulation of polarisation mode dispersion and its effects in long-haul optically amplified lightwave systems. *In IEE Colloquium on International Transmission System*. 1994.

12. **Diez, S.**, **C. Schmidt**, **R. Ludwig**, **H. G. Weber**, **K. Obermann**, **S. Kindt**, **I. Koltchanov**, and **K. Petermann** (1997). Four-wave mixing in semiconductor optical amplifiers for frequency conversion and fast optical switching. *IEEE Journal of selected topics in Quantum Electronics*, **3**(5), 1131–1145.

13. **Dong, P.**, **J. Lee**, **Y.-K. Chen**, **L. L. Buhl**, **S. Chandrasekhar**, **J. H. Sinsky**, and **K. Kim** (2016). Four-channel 100-gb/s per channel discrete multitone modulation using silicon photonic integrated circuits. *Journal of Lightwave Technology*, **34**(1), 79–84.

14. **Doussiere, P.**, **F. Pommerau**, **D. Leclerc**, **R. Ngo**, **M. Goix**, **T. Fillion**, **P. Bousselet**, and **G. Laube**, Polarization independent 1550 nm semiconductor optical amplifier packaged module with 29 db fiber to fiber gain. *In Optical Amplifiers and their Applications*. Optical Society of America, 1995.

15. **Du, L. B.**, **M. M. Morshed**, and **A. J. Lowery** (2012). Fiber nonlinearity compensation for ofdm super-channels using optical phase conjugation. *Optics express*, **20**(18), 19921–19927.

16. **Duthel, T.**, **C. R. S. Fludger**, **J. Geyer**, and **C. Schulien**, Impact of polarisation dependent loss on coherent polmux-nrz-dqpsk. *In OFC/NFOEC 2008 - 2008 Conference on Optical Fiber Communication/National Fiber Optic Engineers Conference*. 2008.

17. **El Gamal, H.** and **M. O. Damen** (2003). Universal space-time coding. *IEEE Transactions on Information Theory*, **49**(5), 1097–1119.

18. **El-Tanany, M. S.**, , and **L. Hazy** (2001). Analytical modeling and simulation of phase noise interference in ofdm-based digital television terrestrial broadcasting systems. *IEEE Transactions on Broadcasting*, **47**(1), 20–31. ISSN 0018-9316.

19. **Ellis, A. D.**, **J. Zhao**, and **D. Cotter** (2010). Approaching the non-linear shannon limit. *Journal of Lightwave Technology*, **28**(4), 423–433.

20. **Essiambre, R.-J.**, **G. J. Foschini**, **G. Kramer**, and **P. J. Winzer** (2008). Capacity limits of information transport in fiber-optic networks. *Physical review letters*, **101**(16), 163901.

21. **Essiambre, R.-J.**, **G. Kramer**, **P. J. Winzer**, **G. J. Foschini**, and **B. Goebel** (2010). Capacity limits of optical fiber networks. *Journal of Lightwave Technology*, **28**(4), 662–701.

22. **Fatadin, I.**, **D. Ives**, and **S. J. Savory** (2014). Carrier phase recovery for 16-qam using qpsk partitioning and sliding window averaging. *IEEE Photonics Technology Letters*, **26**(9), 854–857. ISSN 1041-1135.

23. **Giacoumidis, E.**, **S. Mhatli**, **M. F. Stephens**, **A. Tsokanos**, **J. Wei**, **M. E. McCarthy**, **N. J. Doran**, and **A. D. Ellis** (2017). Reduction of nonlinear intersubcarrier intermixing in coherent optical ofdm by a fast newton-based support vector machine nonlinear equalizer. *Journal of Lightwave Technology*, **35**(12), 2391–2397.

24. **Gordon, J. P.** and **H. Kogelnik** (2000). Pmd fundamentals: Polarization mode dispersion in optical fibers. *Proceedings of the National Academy of Sciences*, **97**(9), 4541–4550. ISSN 0027-8424. URL `https://www.pnas.org/content/97/9/4541`.

25. **Ha, Y.** and **W. Chung** (2013). Non-data-aided phase noise suppression scheme for co-ofdm systems. *IEEE Photonics Technology Letters*, **25**(17), 1703–1706. ISSN 1041-1135.

26. **HARRIS, F. J.**, Chapter 8 - time domain signal processing with the dft. *In* **D. F. Elliott** (ed.), *Handbook of Digital Signal Processing*. Academic Press, San Diego, 1987. ISBN 978-0-08-050780-4, 633 – 699. URL `http://www.sciencedirect.com/science/article/pii/B9780080507804500138`.

27. **Ip, E.** and **J. M. Kahn** (2008). Compensation of dispersion and nonlinear impairments using digital backpropagation. *Journal of Lightwave Technology*, **26**(20), 3416–3425. ISSN 0733-8724.

28. **Juarez, A. A.**, **C. A. Bunge**, **S. Warm**, and **K. Petermann** (2012). Perspectives of principal mode transmission in mode-division-multiplex operation. *Opt. Express*, **20**(13), 13810–13824. URL `http://www.opticsexpress.org/abstract.cfm?URI=oe-20-13-13810`.

29. **Kálmán, R. E.**, A new approach to linear filtering and prediction. 1960.

30. **Kazovsky, L. G.**, **L. Curtis**, **W. C. Young**, and **N. K. Cheung** (1987). All-fiber 90Âř optical hybrid for coherent communications. *Applied optics*, **26**(3), 437–439.

31. **Kolner, B. H.** and **D. W. Dolfi** (1987). Intermodulation distortion and compression in an integrated electrooptic modulator. *Applied Optics*, **26**(17), 3676–3680.

32. **Li, A.**, **X. Chen**, **G. Gao**, and **W. Shieh** (2012). Transmission of 1 tb/s unique-word dft-spread ofdm superchannel over 8000 km edfa-only ssmf link. *Journal of Lightwave Technology*, **30**(24), 3931–3937.

33. **Liu, X.**, **Y. Qiao**, and **Y. Ji** (2010). Reduction of the fiber nonlinearity impairment using optical phase conjugation in 40 gb/s co-ofdm systems. *Optics Communications*, **283**(13), 2749–2753.

34. **Lorattanasane, C.** and **K. Kikuchi** (1997). Design theory of long-distance optical transmission systems using midway optical phase conjugation. *Journal of Lightwave Technology*, **15**(6), 948–955.

35. **Lowery, A. J.** and **J. Armstrong** (2005). 10 gbit/s multimode fiber link using power-efficient orthogonal-frequency-division multiplexing. *Optics Express*, **13**(25), 10003–10009.

36. **Mecozzi, A.** and **M. Shtaif** (2002). The statistics of polarization-dependent loss in optical communication systems. *IEEE Photonics Technology Letters*, **14**(3), 313–315. ISSN 1041-1135.

37. **Morshed, M.**, **L. B. Du**, and **A. J. Lowery** (2013). Mid-span spectral inversion for coherent optical ofdm systems: Fundamental limits to performance. *Journal of Lightwave Technology*, **31**(1), 58–66.

38. **Mousa-Pasandi, M. E.** and **D. V. Plant** (2010). Zero-overhead phase noise compensation via decision-directed phase equalizer for coherent optical ofdm. *Opt. Express*, **18**(20), 20651–20660. URL `http://www.opticsexpress.org/abstract.cfm?URI=oe-18-20-20651`.

39. **Mumtaz, S.**, **G. . Othman**, and **Y. Jaouen**, Space-time codes for optical fiber communication with polarization multiplexing. *In 2010 IEEE International Conference on Communications*. 2010. ISSN 1938-1883.

40. **Naimi, S. T.**, **S. P. Ó. Dúill**, and **L. P. Barry** (2014). Detailed investigation of the pump phase noise tolerance for wavelength conversion of 16-qam signals using fwm. *Journal of Optical Communications and Networking*, **6**(9), 793–800.

41. **Nee, R. v.** and **R. Prasad**, *OFDM for wireless multimedia communications*. Artech House, Inc., 2000.

42. **Omiya, T.**, **M. Yoshida**, and **M. Nakazawa** (2013). 400 gbit/s 256 qam-ofdm transmission over 720 km with a 14 bit/s/hz spectral efficiency by using high-resolution fde. *Optics express*, **21**(3), 2632–2641.

43. **Proakis, J.**, *Digital Communications*. McGraw-Hill series in electrical and computer engineering : communications and signal processing. McGraw-Hill, 2001. ISBN 9780071181839. URL https://books.google.co.in/books?id=aUp2QgAACAAJ.

44. **Qian, D.**, **T. T.-O. Kwok**, **N. Cvijetic**, **J. Hu**, and **T. Wang**, 41.25 gb/s real-time ofdm receiver for variable rate wdm-ofdma-pon transmission. *In Optical Fiber Communication Conference*. Optical Society of America, 2010.

45. **Schawlow, A. L.** and **C. H. Townes** (1958). Infrared and optical masers. *Phys. Rev.*, **112**, 1940–1949. URL https://link.aps.org/doi/10.1103/PhysRev.112.1940.

46. **Serena, P.** (2009). Optilux (version 0.1). URL http://optilux.sourceforge.net. Open source, free software.

47. **Shieh, W.** and **C. Athaudage** (2006). Coherent optical orthogonal frequency division multiplexing. *Electronics letters*, **42**(10), 587–589.

48. **Shieh, W.**, **H. Bao**, and **Y. Tang** (2008). Coherent optical ofdm: theory and design. *Optics express*, **16**(2), 841–859.

49. **Shieh, W.** and **I. Djordjevic**, *OFDM for optical communications*. Academic Press, 2009.

50. **Shieh, W.**, **X. Yi**, **Y. Ma**, and **Y. Tang** (2007). Theoretical and experimental study on pmd-supported transmission using polarization diversity in coherent optical ofdm systems. *Opt. Express*, **15**(16), 9936–9947. URL http://www.opticsexpress.org/abstract.cfm?URI=oe-15-16-9936.

51. **Tanaka, Y.**, **T. Komine**, **S. Haruyama**, and **M. Nakagawa**, Indoor visible communication utilizing plural white leds as lighting. *In 12th IEEE International Symposium on Personal, Indoor and Mobile Radio Communications. PIMRC 2001. Proceedings (Cat. No. 01TH8598)*, volume 2. IEEE, 2001.

52. **Tang, Y.**, **W. Shieh**, **X. Yi**, and **R. Evans** (2007). Optimum design for rf-to-optical up-converter in coherent optical ofdm systems. *IEEE Photonics Technology Letters*, **19**(7), 483–485. ISSN 1041-1135.

53. **Tang, Y.**, **W. Shieh**, **X. Yi**, and **R. Evans** (2007). Optimum design for rf-to-optical up-converter in coherent optical ofdm systems. *IEEE Photonics Technology Letters*, **19**(7), 483–485.

54. **van den Borne, D.**, **V. A. J. M. Sleiffer**, **M. S. Alfiad**, **S. L. Jansen**, and **T. Wuth**, Polmux-qpsk modulation and coherent detection: The challenge of long-haul 100g transmission. *In 2009 35th European Conference on Optical Communication*. 2009. ISSN 1550-381X.

55. **Viterbi, A.** (1983). Nonlinear estimation of psk-modulated carrier phase with application to burst digital transmission. *IEEE Transactions on Information Theory*, **29**(4), 543–551. ISSN 0018-9448.

56. **Warm, S.** and **K. Petermann** (2013). Splice loss requirements in multi-mode fiber mode-division-multiplex transmission links. *Optics Express*, **21**(1), 519–532.

57. **Watanabe, S.** and **M. Shirasaki** (1996). Exact compensation for both chromatic dispersion and kerr effect in a transmission fiber using optical phase conjugation. *Journal of Lightwave Technology*, **14**(3), 243–248.

58. **Winzer, P. J.** (2012). High-spectral-efficiency optical modulation formats. *Journal of Lightwave Technology*, **30**(24), 3824–3835. ISSN 0733-8724.

59. **Wu, S.** and **Y. Bar-Ness** (2004). Ofdm systems in the presence of phase noise: consequences and solutions. *IEEE Transactions on Communications*, **52**(11), 1988–1996. ISSN 0090-6778.

60. **Yi, X.**, **W. Shieh**, and **Y. Tang** (2007). Phase estimation for coherent optical ofdm. *IEEE Photonics Technology Letters*, **19**(12), 919–921. ISSN 1041-1135.

61. **Zibar, D.**, **M. Piels**, **R. Jones**, and **C. G. Schäeffer** (2016). Machine learning techniques in optical communication. *Journal of Lightwave Technology*, **34**(6), 1442–1452.